NOAA Technical Memorandum ERL SEL-39

U.S. DEPARTMENT OF COMMERCE
NATIONAL OCEANIC AND ATMOSPHERIC ADMINISTRATION
Environmental Research Laboratories

Propagation and Detection of Turbulence Generated MHD Waves in the Lower Solar Atmosphere

STEPHEN J. MANGIS

Space Environment Laboratory
BOULDER, COLORADO
February 1975

IMENTAL RESEARCH LABORATORIES

PACE ENVIRONMENT LABORATORY

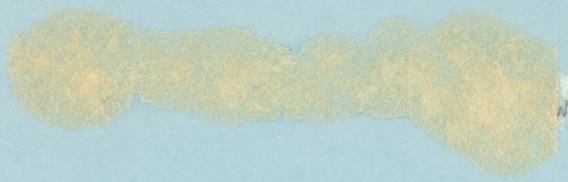

IMPORTANT NOTICE

Technical Memoranda are used to insure prompt dissemination of special studies which, though of interest to the scientific community, may not be ready for formal publication. Since these papers may later be published in a modified form to include more recent information or research results, abstracting, citing, or reproducing this paper in the open literature is not encouraged. Contact the author for additional information on the subject matter discussed in this Memorandum.

NATIONAL OCEANIC AND ATMOSPHERIC ADMINISTRATION

NOAA Technical Memorandum ERL SEL-39

PROPAGATION AND DETECTION OF TURBULENCE GENERATED MHD WAVES IN THE LOWER SOLAR ATMOSPHERE

Stephen J. Mangis

Space Environment Laboratory
Boulder, Colorado
February 1975

UNITED STATES
DEPARTMENT OF COMMERCE
Rogers C.B. Morton, Secretary

NATIONAL OCEANIC AND
ATMOSPHERIC ADMINISTRATION
Robert M. White, Administrator

Environmental Research
Laboratories
Wilmot N. Hess, Director

CONTENTS

SYMBOLS

A	velocity amplitude of a disturbance
B	magnetic field strength
C	local sound speed
c	speed of light
E	electric field strength
H	scale height
k	wavenumber
K	Boltzman constant
R	solar radius
T	temperature; wave period
u	turbulent velocity amplitude
V	velocity
μ	refractive index; magnetic permeability
θ	angle of incidence; angle between direction of wave propagation and magnetic field
λ	wavelength
ρ	density
ω_ρ	plasma frequency
σ	electrical conductivity
τ	decay time
χ	excitation potential

PROPAGATION AND DETECTION OF TURBULENCE GENERATED MHD WAVES IN THE LOWER SOLAR ATMOSPHERE

Stephen J. Mangis

Some basic solar concepts are developed and the limiting effects of the terrestrial atmosphere upon solar observations are investigated. Some theoretical aspects of MHD waves and the frequency spectrum of MHD waves generated by the hydrogen convection zone are discussed. The magnitudes of various observable characteristics of these waves are calculated, and there is a brief discussion of how we hope to observe these characteristics.

We conclude that the visual changes caused by turbulence generated MHD waves are of sufficient magnitude to be observed by orbiting telescopes now being developed, but that more work needs to be done to determine exactly how and where to observe these changes.

Key Words: Sun, MHD waves, large orbiting telescope.

1. INTRODUCTION

The Sun has been an object of study since earliest history because of the immense importance of solar radiation in the everyday life of man. In the twentieth century, however, man has come to realize that the Sun is important for far more than its light and heat: the Sun is of great intrinsic interest as the only nearby star, and one which may therefore help unlock the secrets of the universe; the Sun has a great effect on the planets, and in particular on Earth and the human race; and the Sun can be a very valuable astrophysical laboratory, where physical processes unattainable on Earth can proceed with ease.

The Sun indeed occupies a unique place in stellar astronomy. It is the only star on which disk features can be resolved. Spectral scans from disk center to limb yield information that allows determination of temperature and density gradients in the lower atmosphere. This model solar atmosphere is then available for use as a standard against which

atmospheric and spectral line observations of other stars can be compared. Stellar activity cycles can be studied in detail only on the Sun.[1]* Also, the Sun is a stable, main sequence star[2], and as such serves as a standard for stellar photometry and spectroscopy. In addition, if one assumes that He and D abundances have remained essentially constant in the solar atmosphere since the birth of the Sun (Brandt, 1966), determination of these abundances could give a fairly accurate model for relative abundances immediately following a "big bang" creation of the universe.

Knowledge of the Sun not only contributes to our understanding of stellar physics, but to our understanding of planetary physics as well. Solar radiation causes dissociation, excitation, and ionization of atoms and molecules in planetary atmospheres, produces ionospheres, maintains planetary heat budgets, contributes to escape of atmospheres from the planets, is largely responsible for climate, and controls virtually all life forms as we know them. Solar particle fluxes affect planetary ionospheres and magnetic fields, produce aurorae, and fill the interplanetary regions.

Solar-terrestrial and solar-biological relations are, of course, of prime importance. Recent evidence indicates that geomagnetic storms induced by solar activity may affect long range terrestrial weather patterns, and statistical evidence[3] is beginning to suggest that geomagnetic storms may also have profound biological impact. Man in space is veritably at the mercy of unusually energetic solar activity, as the events of August 1972[4] so dramatically indicated. During solar maximum several series of events, each as energetic as those of August 1972, may occur per year, so that manned space flights may have to be timed to coincide with the low periods in the solar activity cycle. In addition, communication by electromagnetic radiation is strongly affected by highly energetic solar events.

That the Sun can be a valuable astrophysical laboratory has been evident ever since Janssen's discovery of helium[5], and Edlen[6] has used coronal emissions to precisely determine otherwise inaccessible atomic parameters. The temperatures, densities, and path lengths found on the

---

*Footnotes appear in Section 5.

Sun favor many plasma and magnetohydrodynamic processes that are difficult if not impossible to duplicate on Earth. If it were possible to observe such processes in sufficient detail, progress might be made toward such pressing problems as controlled use of nuclear fusion.

1.1 Atmospheric Limitations

Unfortunately, it is not possible to study many solar phenomena in sufficient detail from ground-based observatories because of the perturbing effects of the terrestrial atmosphere. Of the total solar flux falling on the terrestrial atmosphere, an average of 40 percent is reflected back into space. Of the 60 percent which does penetrate into the atmosphere, another 15 percent is absorbed, so that only about 45 percent of the incident solar flux reaches the ground. The atmospheric gases effectively block all solar radiation shorter than about 2900Å, and it is this part of the ultraviolet and X-ray spectra that contains the resonance lines[7] of most elements; that is emitted by the transition region[8]; that contains many of the strongest coronal lines; and that contains the largest variations of radiation flux with activity. This part of the spectrum has been explored somewhat by the ATM experiments on board SKYLAB, and by the VELA, OSO, and Solrad satellites.

In addition to absorbing short wavelengths, the Earth's atmosphere is also responsible for severely distorting images in those wavelengths it does allow to pass. The best practical resolution for ground-based observations is about 0.5 arcsec for photographs and 0.8 arcsec for spectra, although this limit is achieved only rarely and only with the best seeing.

The X-ray and very short ultraviolet components of the solar spectrum are absorbed in the upper atmosphere, chiefly because of ionization of O_2 and N_2 leading to O_2^+, N_2^+, and O^+. Owing to mixing, the ozone forming reaction

$$O + O_2 + O_2 \rightarrow O_3 + O_2$$

can then take place, and an ozone layer is built up. It is this ozone layer that effectively blocks all radiation shorter than about 2900Å.

The terrestrial atmosphere also restricts transmission at the infrared (IR) end of the spectrum. Ozone absorbs in narrow bands centered at 9.6, 4.7, and 14.2μ. Carbon dioxide in the atmosphere is a powerful absorber of IR, in narrow bands at 2.7 and 4.3μ, and from 13 to 17μ. Water vapor is the strongest IR absorber in our atmosphere, with strong absorption bands centered at 1.4, 1.85, 2.7, and 6.3μ, and a wide rotational band[9] from 14μ to 1 mm. Figure 1 shows the severe distortion of the solar spectrum due to terrestrial atmospheric absorption.

Scattering in the terrestrial atmosphere is also a great problem to solar observations, especially observations of the corona. As shown in figure 2, the intensity of the clear blue sky is greater than almost all coronal emissions. This blue sky is a consequence of Rayleigh scattering, that is, scattering of incident solar radiation by small particles in the Earth's atmosphere. Rayleigh scattering is also unfortunate in that it induces an unwanted polarization factor.

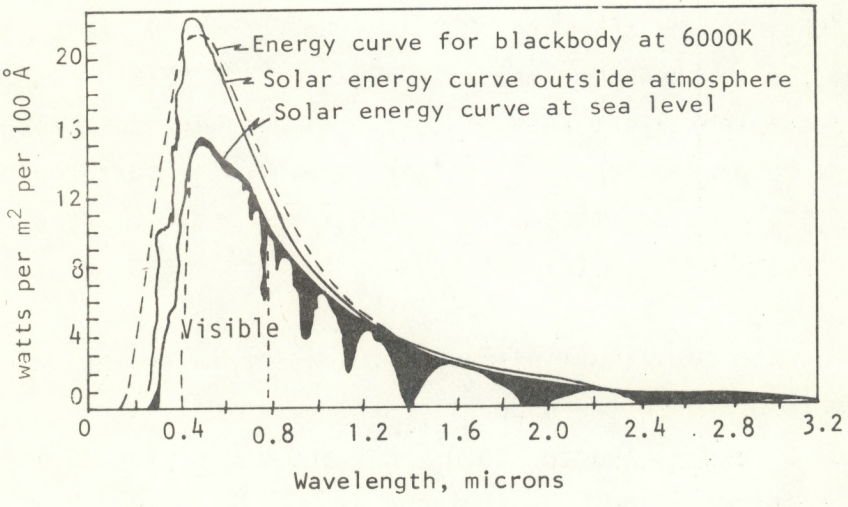

Figure 1. Spectral energy curve of the Sun at sea level and outside the atmosphere after Brandt (1966).

In addition to absorbing and scattering solar radiation, the atmosphere severely distorts the radiation that it does allow to pass. To understand this process we start with Snell's law

$$\mu \sin\theta = \text{constant}$$

where μ = refractive index, θ = angle of incidence.

Differentiating, following Menzel (1961)

$$d\mu/\mu = d\theta \ln\mu = \cot\theta d\theta \quad . \tag{1}$$

We know that for any function ψ(ψ a function of x,y, and z only)

$$d\psi = \frac{\partial\psi}{\partial x} dx + \frac{\partial\psi}{\partial y} dy + \frac{\partial\psi}{\partial z} dz$$

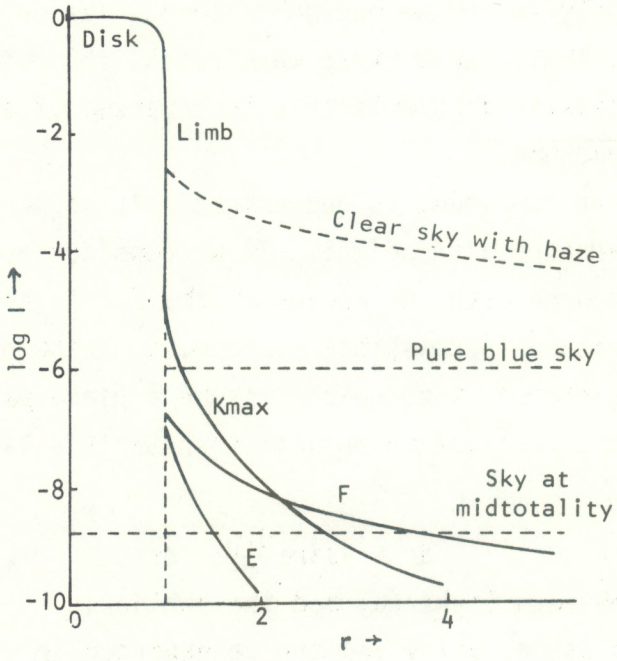

Figure 2. Relative intensities of the components of the coronal spectrum compared with sky brightening after Brandt (1966).

and if $d\underline{s}$ is an element of an incident ray

$$d\psi = d\underline{s} \cdot \nabla\psi = |\nabla\psi| \; d\underline{s} \cos\theta \quad .$$

If we let $\psi = \ln\mu$ then (1) shows that the incident ray suffers a deflection $d\theta$ such that

$$d\theta = -\tan\theta \; d\underline{s} \cdot \nabla\ln\mu = -\sin\theta \cdot |\nabla\ln\mu| d\underline{s} \; . \qquad (2)$$

Equation (2) is general, since the refractive index is free to vary from point to point and $\nabla\ln\mu$ may change continuously in magnitude and direction. Now, we also know that the refractive index of a gas is given by Ingard and Kraushaar (1966)

$$\mu = 1 + (\mu_o - 1)q$$

$$(\mu_o - 1) = (287.5 + \frac{1.3}{\lambda^2} + \frac{.03}{\lambda^4}) \times 10^{-6}$$

where q is the ratio between the actual density and the density at STP (760 mm Hg and 273°K) and λ is in microns. This quantity does depend on wavelength, but only in the second order terms. We can therefore see, from (1) and (2), that, for a given wavelength, the deflection depends on the atmospheric density gradient; this is composed of a systematic and a fluctuating component.

The systematic component is due essentially to the variation of density and temperature with height. If we consider for a moment path lengths short compared with the radius of the Earth, to allow us to ignore Earth curvature (permissible since most of the density gradient occurs near the surface), then we can assume a plane parallel atmosphere. If z is the vertical coordinate then Snell's law gives

$$d\alpha = -\sin\alpha \frac{d\ln\mu}{dz} \; ds \qquad (3)$$

where α = angle between light ray and the vertical.

Since μ is close to unity $\ln\mu$ can be expanded in a McLaurin series[10]

$$\ln\mu = (\mu_o - 1)q$$

and

$$\frac{d\ln\mu}{dz} = (\mu_o - 1)\frac{dq}{dz} = -a(\mu_o - 1)e^{-ah} \qquad (4)$$

where h = height.

Since we are restricting ourselves to small path lengths and therefore small deflections we can integrate (3) and hold $\sin\alpha$ on the right constant:

$$\Delta\alpha = -\sin\alpha \frac{d\ln\mu}{dz} \; l$$

where $\Delta\alpha$ = deflection for total path length l.

Substituting into (4)

$$\Delta\alpha = a(\mu_o - 1)e^{-ah}(\sin\alpha)\, l \quad .$$

This expresses the deflection in radians. Putting in numbers and converting to seconds of arc (1 rad - 206265 arcsec), we have

$$\Delta\alpha = 6e^{-0.1h}\, l \sin\alpha \text{ arcsec}$$

where h and l are in km. For a path length of, say, 100 m at sea level

$$\Delta\alpha = 0.6 \sin\alpha \quad .$$

The maximum deflection occurs for $\sin\alpha = 1$ (horizontal rays) and amounts to about 0.6 arcsec. Since we have considered only short path lengths, deflection due to the systematic component of the density gradient will be greater than 0.6 arcsec for all but the most exceptional cases.

To this effect must be added the effect of the fluctuating component of the density gradient. This is due to local heating and cooling, wind turbulence, weather effects, and the like. A mass of hot or cool air can give rise to much greater deflection than the systematic conditions described above.

Since air is compressible, only momentary pressure changes will result from local heating and cooling. The chief effect will be a density change, and for isobaric conditions we have

$$\frac{\Delta\rho}{\rho} = \frac{\Delta T}{T}$$

where ρ = density, T = temperature.

Since temperature and density will change along a light ray traversing this mass of air, the refractive index will also change. Applying the theorem of the mean[11] to (1),

$$\cot\vartheta\Delta\theta = \frac{\Delta\mu}{\mu} \quad .$$

(Here we have changed from differentials to finite differences; this is valid for small increments.) $\Delta\theta$ is the total deflection and $\Delta\mu$ is the variation in refractive index from the mean (systematic) value. θ is the average value of the angle between the light ray and the direction of the density gradient. Since the mean value of $\cot\theta$ over a hemisphere is 1, we have

$$\frac{\Delta\mu}{\mu} = (\mu_o - 1)\frac{\Delta\rho}{\rho}$$

and

$$\frac{\Delta\mu}{\mu} = -(\mu_o - 1)\frac{\Delta T}{T}$$

so the expected deflection is

$$|\Delta\theta| = (\mu_o - 1)\frac{\Delta T}{T}. \quad .$$

For example, if $\Delta T=30°C$, $T=15°C$, and $C=283°K$, then $\Delta T/T \simeq 0.1$ and $\Delta\theta = 0.00029 \times 0.1 \times 206265 = 6$ arcsec.

This temperature difference is fairly extreme, so a more commonly encountered deflection may be more of the order of 4 arcsec. It should be remembered, however, that this is due to a single deflection. In traversing the atmosphere, a ray will undergo many successive deflections. If there are N deflecting elements in the path, the total deflection will be of the order $N^{\frac{1}{2}}$ times the magnitude of an individual deflection. (This is the random walk problem; see for example, Feyman, 1963.) For, say, 10 such elements, each deflecting 4 arcsec (extremely poor seeing), we have a total of some 12 arcsec deflection. The

inevitable result is that the image of a point source will be blurred or will shimmer, and explains why seeing at proposed observatory sites must be carefully studied.

Weather also contributes to atmospheric limitations. Various synoptic observation programs have the scales of hours, days, or even weeks, depending on the solar feature whose development they are trying to trace. Clouds and weather systems of course severely limit the ability of ground-based observatories to carry out such observations.

Since even high flying balloons are limited to about 0.2 arcsec resolution (Nat. Acad. Sci., 1966), the obvious solution to the problems imposed by atmospheric restrictions is to place solar telescopes above the atmosphere, in Earth orbit. This was done on SKYLAB with great success. Unfortunately, to date no high resolution systems capable of taking full advantage of the complete lack of atmospheric distortion have been orbited. There are, however, many unanswered questions in solar physics -- including MHD wave propagation -- that demand the higher resolution available only from an orbiting telescope. Before going into the physics of MHD waves, however, it is appropriate to examine in a general way the structure of the solar atmosphere and the processes that give rise to hydrogen convection zone turbulence.

1.2 Convection Zone Turbulence

All of the energy that is eventually released at the solar surface was originally liberated in the solar interior by fusion processes. Two such processes are thought to be important — the carbon cycle and the proton-proton chain. In the carbon cycle, $4H^1$ are transformed into the $1He^4$ with C^{12} acting as a catalyst:

$$C^{12} + H^1 \rightarrow N^{13} + \gamma$$
$$N^{13} \rightarrow C^{13} + e^+ + \text{neutrino}$$
$$C^{13} + H^1 \rightarrow N^{14} + \gamma$$
$$N^{14} + H^1 \rightarrow O^{15} + \gamma$$
$$O^{15} \rightarrow N^{15} + e^+ + \text{neutrino}$$
$$N^{15} + H^1 \rightarrow C^{12} + He^4 \quad .$$

In the proton-proton chain, $4H^1$ are again transformed into $1He^4$, but by a different route:

$$H^1 + H^1 \rightarrow D^2 + e^+ + \text{neutrino}$$
$$D^2 + H^1 \rightarrow He^3 + \gamma$$
$$He^3 + He^3 \rightarrow He^4 + H^1 + H^1 \ .$$

The total energy released per He atom formed is roughly the same for each process (4×10^{-5} erg versus 4.3×10^{-5} erg), but each process reacts quite differently to temperature. For the temperature believed to exist in the core of the Sun, the proton-proton chain is dominant, but both are important (see fig. 3).

The energy liberated in the core travels outward by radiation. Temperature, pressure, density, and the average energy of a photon all decrease with increasing distance from the center. Photons are absorbed and re-emitted many times as they diffuse outward, and in this way the gamma rays generated in the core are changed to X-rays, then XUV rays, UV rays, and finally to visible light. At about 0.86R, the temperature and density

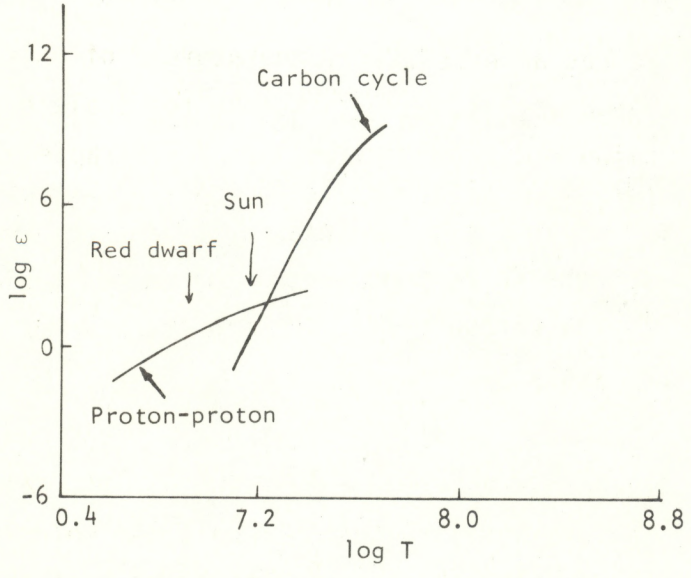

Figure 3. Energy liberation rates as a function of temperature for stellar conditions, after Brandt (1966).

structure is such that the gas has become unstable to convection, so some energy is transported outward from this point by turbulent convection.

This convection layer arises because the prevailing temperature has by this point become much lower than that in the core. Because of this, a significant fraction of the free electrons in the gas are moving slowly enough that they can be captured by hydrogen nuclei to form atoms. This increases the opacity of the gas, and, since photons are more easily absorbed by the atoms, the resistance to radiation diffusion is increased. As a result the temperature gradient steepens, which leads directly to the Schwarzschild instability criterion[12] being satisfied.

As density, temperature, and pressure continue to decrease (moving outward) a layer is finally reached where a photon emitted outward has only a small probability of being reabsorbed or scattered, and in fact is more likely to escape into space after passing through the essentially transparent overlying atmosphere. This layer is called the photosphere and is the lowest layer of the solar atmosphere to which we can see.

1.3 The Solar Atmosphere

1.3.1 The Photosphere

The photosphere has an effective temperature[13] of only about 5780°K. Since the Sun is in hydrostatic equilibrium[14], the scale height[15] is small and the density, moving radially outward, decreases rapidly. The negative hydrogen ion (H^-) density therefore also decreases rapidly, and, since H^- generates most of the absorption and emission at visible wavelengths, the radiation we see comes from a thin layer only some 100 km thick. As this is only 0.014R, the visible Sun appears to have a very sharp limb, as opposed to the radio or X-ray Sun. The region called the photosphere is generally defined as being about 500 km thick and radiates almost all the energy emitted by the Sun. It is probably no accident of molecular evolution that almost half the solar energy reaching Earth lies in the wavelength range to which our eyes are sensitive (see fig.1).

Photons of all energies are emitted by the photosphere; a true white light spectrum is generated. However, if the energy of a photon in

the white light spectrum is close to an electron transition energy of one of the elements in the solar atmosphere above the photosphere, the photon stands a greatly increased probability of being absorbed and re-emitted at a different frequency, in a different direction, or both. The result is that we do not see a true white light spectrum, but rather a spectrum that includes absorption lines[16]. Since radiation from off line center will have a lower probability of being absorbed, we can effectively see to various layers in the solar atmosphere by studying various wavelengths. If, however, we choose to study the Sun in white light, without any special filters restricting us to narrow wavelength ranges, many beautiful and intriguing photospheric phenomena immediately become apparent.

The most intriguing of the photospheric features, and one which has puzzled men since the time of Galileo, is sunspots. Sunspots are large, dark spots (fig. 4) that appear and disappear at unpredictable places and times on the solar surface, and are closely related by as yet unknown mechanisms to large, energetic chromospheric solar eruptions known as flares. Sunspots can be many times larger than the Earth and may persist for as long as several months.

Granulation is another photospheric phenomenon, but one which is much smaller than sunspots. Granulation is thought to be a manifestation of convection from the hydrogen convection zone. Resembling a layer of corn kernels, the observed granulation pattern really consists of the tops of convection cells which bubble up from beneath the photosphere, radiate away their excess heat, and then sink back beneath the surface. Average cell lifetime is about 10 min, but since their average diameter is about 1800 km (2 arcsec) (Gibson, 1973), it is impossible to study these cells from the ground without excellent seeing.

Larger cells, called supergranules, have also been observed. These are about 18 times as large as granules, persist about 120 times as long, and are thought to be strongly connected with the chromospheric network (see fig. 5).

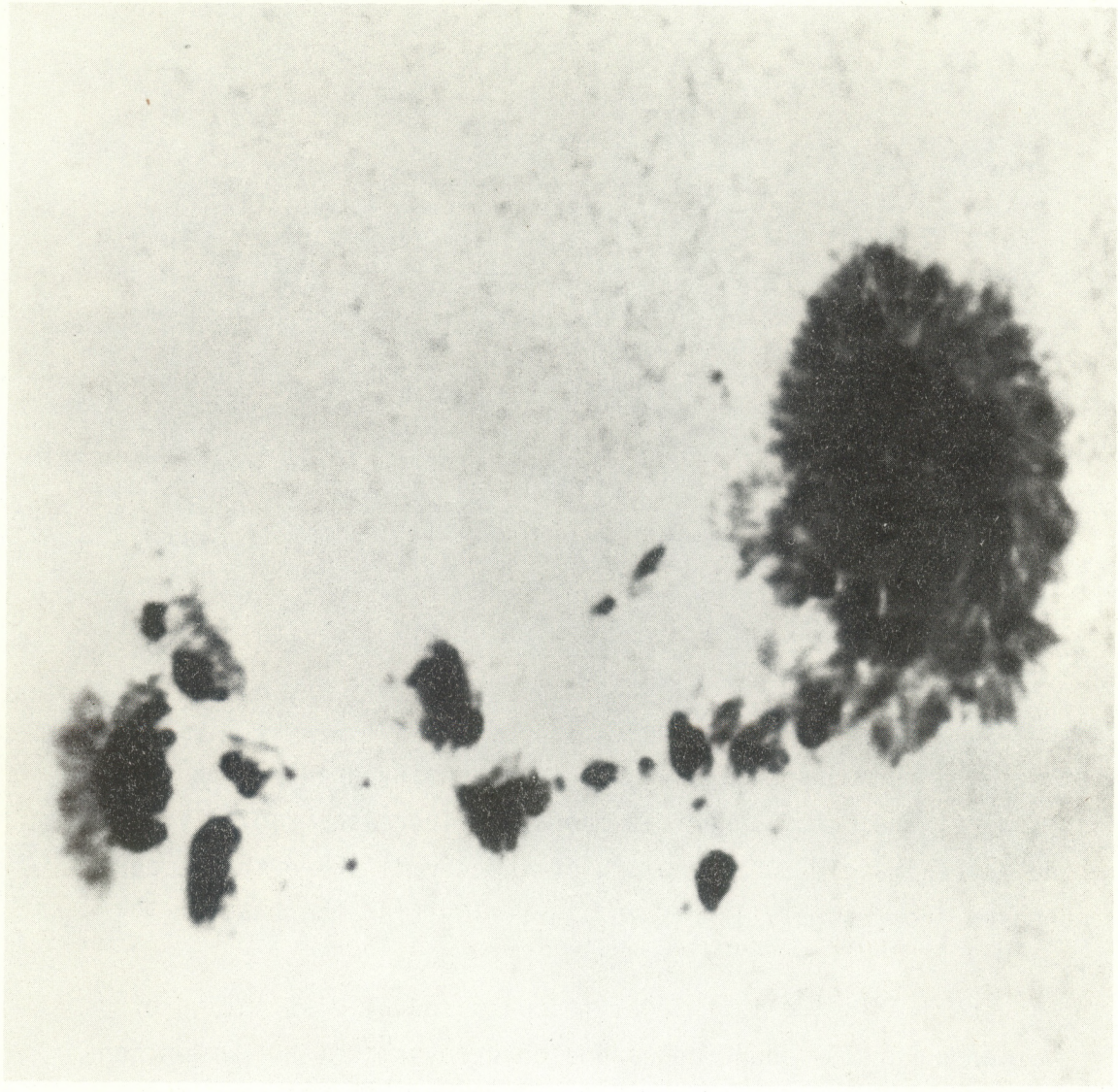

Figure 4. White light photograph of the Sun showing sunspots.

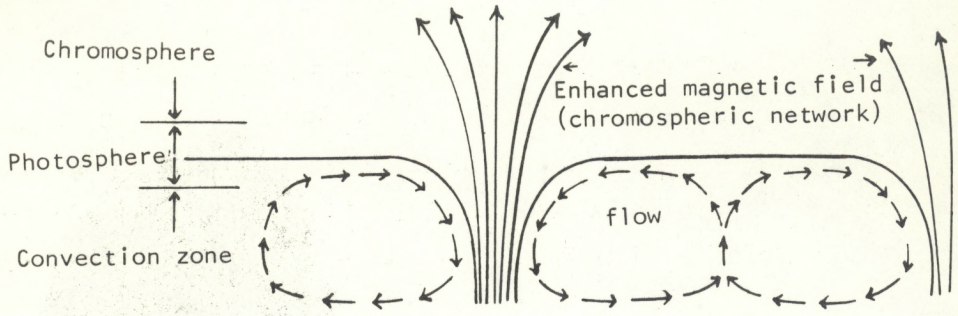

Figure 5. Supergranular flow and enhanced magnetic field strength in the chromospheric network, after Gibson (1975).

1.3.2 The Chromosphere

Immediately above the photosphere lies the chromosphere. Like the photosphere, the chromosphere has a negative density gradient, but unlike the photosphere, the chromospheric temperature increases radially outward. Within the approximately 3000 km width of the chromosphere the temperature increases from roughly 4300°K to nearly 10^6°K at the base of the corona.

Chromospheric heating is thought to be caused by dissipation of energy carried upward by sound and magnetohydrodynamic (MHD) waves generated in the rather turbulent photosphere. Gibson has likened the chromosphere to a "froth on top of the turbulent and relatively dense photosphere." If supergranules sweep flux tubes to their boundaries as has been suggested, then these flux tubes would extend up into the chromosphere and magnetically couple this region to the turbulence in the photosphere and convection zone.

In spite of the dynamic character of waves bursting upward through the chromosphere and depositing large amounts of energy there, observations of this region indicate structurally complex phenomena that can be rather stable, e.g., the fibril patterns seen in H-alpha[17] around action regions[18]. This stability is due largely to the low material

density. The kinetic energy of fluid motion is small compared with the magnetic energy density, so the magnetic fields can effectively constrain particle motion. Figure 6 shows an example of chromospheric fine structure.

The boundaries of supergranules are also of interest because it is from these areas that brilliant jets of luminous gas, called spicules, shoot upward some 10,000 km. Spicules, which have a lifetime of 2 to 5 min and a diameter of about 800 km (or about 1 arcsec), may well be a primary mechanism for the flow of energy and material into the corona.

1.3.3 The Corona

The corona is a very tenuous halo that extends outward from the chromosphere to well beyond the radius of the Earth's orbit. The white light coronal spectrum can be broken down into three components. The K corona (from kontinuierlich, German for continuous) is caused by photospheric emission scattered by coronal free electrons and makes up most of

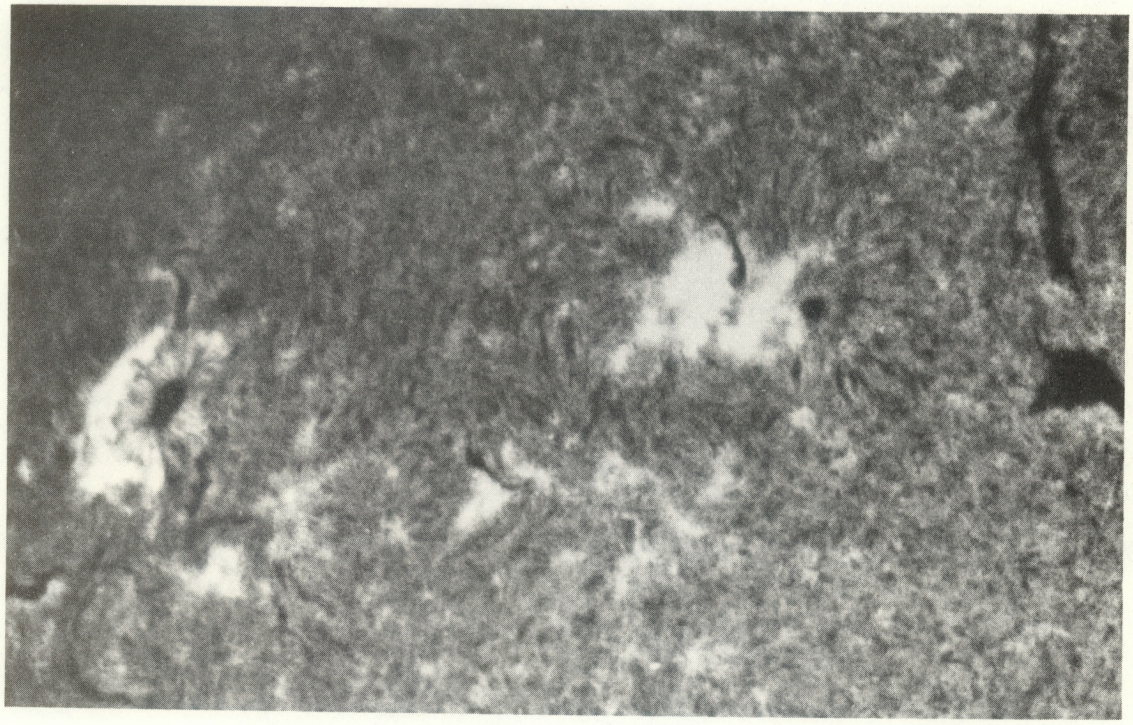

Figure 6. H-alpha photograph showing chromospheric fine structure.

the coronal intensity out to 1.3R (Gibson, 1973). The F corona is due to photospheric radiation being scattered by heavier, slower particles between the Earth and the Sun. Fraunhofer lines do not appear in the K corona because the Doppler shift given the protons by rapidly moving electrons is large enough to smear out the line profiles, whereas heavier particles contribute much smaller Doppler shifts so the F corona does exhibit Fraunhofer lines, although somewhat degraded. The E corona is the final component and is due to high temperature emission lines from coronal ions.

The average coronal temperature is some 1.6×10^6°K, and the corona is therefore essentially a fully ionized plasma (except for heavy ions). The number density is of the order of 3×10^8 cm^{-3} (at about 1.1R), which leads to a "self collision frequency" (after Spitzer, 1962) of γ_e = 11/sec for electrons and γ_p = 0.3/sec for protons and a mean free path of the order of 10^8 cm for both electrons and protons. The plasma frequency $(\omega = 4\pi ne^2/m_e)^{\frac{1}{2}}$ is about 10^9 sec^{-1} and the corresponding Debye distance[19] is about 0.5 cm. Assuming a magnetic field of 4 gauss, the gyrofrequency and gyroradii for electrons are 0.7×10^8 sec^{-1} and 12 cm, respectively, and for protons are 0.4×10^5 sec^{-1} and 5.2×10^3 cm.

One result of coronal high temperature worth exploring in detail because of its relevance to MHD waves is that the magnetic field lines are frozen into the plasma. The electrical conductivity of a fully ionized gas is on the order $\sigma = ne^2/m_e\gamma_e$, and an approximate value for τ, the decay time of an electrical current system in the corona, can be found by dividing the energy density in the magnetic field $(B^2/8\pi)$ by the rate of Ohmic dissipation[20] j^2/σ. Since $j = cB/4\pi L$ (L is a length characteristic of the system), we have $\tau = 4\pi\sigma L^2/c^2$. For L = 10^8 cm, $\tau = 3 \times 10^5$ years, so for observable changes the corona can be considered an ideal conductor. Therefore, Ohm's law can be written (using gaussian system for clarity; later in the paper we will use cgs for ease of computation)

$$0 = \underline{j}/\sigma = \underline{E} + (\underline{v}/c) \times \underline{B} \quad .$$

Also, from Maxwell's equations we have

$$\underline{\nabla} \times \underline{E} = - \frac{1}{c} \frac{\partial B}{\partial t} \quad ,$$

so

$$- \frac{1}{c} \frac{\partial B}{\partial t} = - \underline{\nabla} \times (\frac{v}{c} \times \underline{B}) \quad ,$$

or

$$\frac{\partial B}{\partial t} = - \underline{\nabla} \times (\underline{v} \times \underline{B}) \quad ,$$

which says that the magnetic flux ϕ through an area S is conserved, as we will now prove.

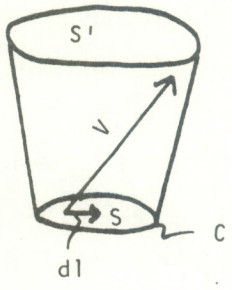

Now, $\phi = \int_S \underline{B} \cdot d\underline{s}$. The rate of change of ϕ with time is due to, first, the surface S moving to S' because of fluid motion, and second, a change of B with time. These are, respectively, $- \int_C \underline{B} \cdot (d\underline{l} \times \underline{v})$ (the flux that passes through S but which escapes out the "sides" and doesn't pass through S') and $\int_S \frac{\partial B}{\partial t} \cdot d\underline{s}$. Using Stokes' theorem[21], we have

$$\frac{d\phi}{dt} = \int_S \left[\frac{\partial B}{\partial t} \cdot \underline{\nabla} \times (\underline{v} \times \underline{B}) \right] \cdot d\underline{s} = 0 \ .$$

In other words, the flux through the walls of a magnetic tube of force is always zero, that is, the field is "frozen into" the plasma. We also know that the ratio of gas pressure to magnetic pressure is

$\beta = \frac{nKT}{B^2/8\pi}$, so, assuming a general field of 4 gauss and the values of n

and T given above, $\beta \simeq 0.2$. We can therefore conclude that the coronal plasma is effectively constrained by the field.

2. MHD WAVES

2.1 Theoretical Considerations

In the introduction we briefly discussed the convection zone and the various layers in the solar atmosphere and showed that the terrestrial atmosphere has a severe distorting effect upon the solar spectrum and, therefore, upon our understanding of the ongoing processes in these various layers. In this section we will examine one process common to all layers in the solar atmosphere and will suggest how to study this process in spite of its small-scale manifestations and the perturbing effects of the terrestrial atmosphere.

The process we have chosen to single out from the many which deserve high resolution study is the propagation of magnetohydrodynamic waves generated by convection zone turbulence. MHD waves are of importance in solar studies for several reasons. First, MHD waves in the Alfvén mode may be responsible for the generation of high speed streams in the solar wind (Hollweg, 1972a). These high speed streams probably are important in causing geomagnetic disturbances and also may heat the upper terrestrial atmosphere and play a part in determining Earth weather patterns (Wilcox, 1973a,b). Also, Alfvén waves have been observed in the solar wind (Belcher and Davis, 1971), and further observation and study could identify the source of these waves in the solar atmosphere. In addition, MHD waves are difficult to study in simulated environments, and study of these waves in the Sun could well contribute to our understanding of MHD wave propagation in perfectly conducting, inhomogeneous plasmas (Hollweg, 1972c) which are typical of astrophysical problems but which are difficult to simulate in the laboratory. Perhaps of greatest significance, however, is the role MHD waves play in heating the solar atmosphere. Osterbrock (1961) has shown that this effect may be quite important and has estimated the possible energy dissipation for a magnetic field of 2 gauss, as shown in table 1.

*Table 1. Energy Dissipation in the Solar Atmosphere For a Magnetic Field of 2 Gauss.**

Height (km)	Area	Energy (erg/cm^2-sec)	Mechanism
100,000	Inner corona	2×10^4	Slow mode shocks
2500	Upper chromosphere	8×10^5	Fast mode waves
1000	Middle chromosphere	6×10^6	Fast mode waves
500	Photosphere and low chromosphere	2×10^7	Fast mode waves
0			

* From Osterbrock (1961).

We turn now to the mechanics of MHD wave propagation. It has been shown that various wave modes propagate in plasma environments (Alfvén and Falthammar, 1963), and this discussion will consider the general case of wave motion in a stationary, compressible, uniform gas of infinite electrical conductivity permeated by a uniform magnetic field which is inclined with respect to the direction of wave propagation. Assume a plane wave propagating in the positive z direction and a magnetic field B_o inclined at an angle θ to the z axis and lying in the y-z plane (see fig. 7). The components of B along the axis are than 0, $B_o \sin\theta$, $B_o \cos\theta$. If we let $d\rho$ and dp be the variations in local density and pressure due to the wave, then the linearized equation of motion is (in cgs system)

$$\rho_o \frac{\partial \underline{v}}{\partial t} = - \underline{\nabla}(dp) + \frac{1}{\mu} (\underline{\nabla} \times \underline{b}) \times \underline{B}_o \ , \qquad (A)$$

where $\underline{b}$ is the variation in the magnetic field due to the wave and $\underline{v}$ is the fluid velocity. If we further assume an adiabatic regime, the variations in pressure and density are related by

$$dp = \frac{\gamma P_o d\rho}{\rho_o} \quad C^2 \, d\rho$$

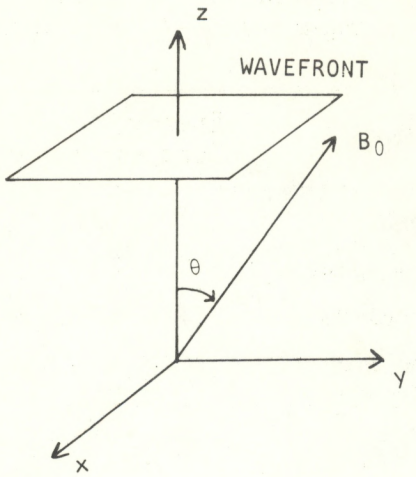

Figure 7. Plane wavefront propagating along the z axis. Uniform magnetic field B_o.

where γ is the ratio of specific heats and C is the sound velocity in the gas. Substituting in A for dp yields

$$\rho_o \frac{\partial \underline{v}}{\partial t} + C^2 \underline{\nabla}(d\rho) - \frac{1}{\mu} (\underline{\nabla} \times \underline{b}) \times \underline{B}_o = 0 \quad . \tag{B}$$

Now, in this regime the (linearized) equation of continuity is

$$\frac{\partial (d\rho)}{\partial t} + \rho \nabla \cdot \underline{v} = 0 \quad , \tag{C}$$

and the equation for conservation of magnetic flux is

$$\frac{\partial \underline{b}}{\partial t} - \underline{\nabla} \times (\underline{v} \times \underline{B}_o) = 0 \quad . \tag{D}$$

Assuming that all variables depend on z and t only, the Maxwell relation div $\underline{b}$ = 0 immediately yields b_z = 0. Breaking (D) and (B) into their components likewise yields

$$\frac{\partial b_x}{\partial t} = (B_o \cos\theta) \frac{\partial v_x}{\partial z} \quad , \tag{D1}$$

$$\frac{\partial b_y}{\partial t} = (B_o \cos\theta) \frac{\partial v_y}{\partial z} - B_o (\sin\theta) \frac{\partial v_z}{\partial z} \quad , \tag{D2}$$

$$\rho \frac{\partial v_x}{\partial t} = (B_o \frac{\cos\theta}{\mu}) \frac{\partial b_x}{\partial z} \quad , \tag{B1}$$

$$\rho \frac{\partial v_y}{\partial t} = (B_o \frac{\cos\theta}{\mu}) \frac{\partial b_y}{\partial z} \quad , \tag{B2}$$

$$\rho \frac{\partial v_z}{\partial t} + C^2 \frac{\partial (d\rho)}{\partial z} + (B_o \frac{\sin\partial}{\mu}) \frac{\partial b_y}{\partial z} = 0 \quad , \tag{B3}$$

and (C) gives

$$\frac{\partial (d\rho)}{\partial t} + \rho_o \frac{\partial v_z}{\partial z} = 0 \quad . \tag{C1}$$

Combining (D1) and (B1) shows that b_x and v_x both satisfy

$$(\frac{\partial^2}{t^2} - \frac{B_o \cos^2\theta}{\mu\rho_o} \frac{\partial^2}{z^2}) \ (b_x, v_x) = 0 \tag{E}$$

This is more typically written with

$$\frac{B_o^2 \cos^2\theta}{\mu\rho_o} = V_z^2 \equiv V_A^2 \cos^2\theta$$

where V_A is called the Alfvén speed.

Combining (D2), (B2), (B3), and (C1) allows us to determine the remaining variables v_y, v_z, b_y, and d. If we consider harmonic waves with frequency $\omega/2\pi$ and wave number k, then all variables go as $\exp\{i(\omega t - kz)\}$, and this mathematical formalism allows us to replace the operators $\partial/\partial t$ and $\partial/\partial z$ with $i\omega$ and $-ik$. We then obtain (Ferraro and Plumpton, 1966)

$$(kB_o \cos\theta)v_y - (kB_o \sin\theta)v_z + \omega b_y = 0,$$

$$\rho_o \omega v_y + (\frac{kB_o \cos\theta}{\mu}) \ b_y = 0 \ ,$$

$$\rho_o \omega v_z + \left(\frac{kB_o \sin\theta}{\mu}\right) b_y - kC^2 \, d\rho = 0 \, ,$$

$$\rho_o \, kv_z + \omega d\rho = 0 \, .$$

Eliminating ratios and combining yields the frequency relation

$$\left(\frac{\omega}{k}\right)^4 - (V_A^2 + C^2)\left(\frac{\omega}{k}\right)^2 + V_A^2 \, C^2 \cos^2\theta = 0 \, . \qquad \text{(F)}$$

Since ω/k is the phase velocity, we define $\omega/k \equiv U$ and rewrite (F)

$$U^4 - (V_A^2 + C^2)U^2 + V_A^2 \, C^2 \cos^2\theta = 0 \qquad \text{(F1)}$$

which can be rearranged as

$$(U^2 - C^2)(U^2 - V_A^2) = C^2 \, V_A^2 \, \sin^2\theta \, . \qquad \text{(F2)}$$

There are four solutions to this equation representing two modes. The case $\theta = 0$ is degenerate with the Alfvén mode given by (wave) eq. (E). For $\theta = \pi/2$, we have $U = \pm \{(V_A^2 + C^2)\}^{\frac{1}{2}}$, which represents a magneto-acoustic wave propagating perpendicular to the magnetic field.

When θ has any value other than 0 or $\pi/2$ one root, U_1^2 will exceed the greater of C^2 and V_A^2 and the other root, U_2^2, will be less than the smaller of C^2 and V_A^2. The former is called the fast mode and the latter the slow mode.

The relative velocities of Alfvén, fast, and slow modes can best be understood by a Friedrichs hodograph. Figure 8 shows two cases, $V_A < C$ and $V_A > C$. In these diagrams, vector $\underline{ov}$, drawn from the origin to a point on one of the curves, represents the velocity and direction of propagation of the wave, the angle θ being the angle between the direction of B_o and the direction of propagation. The three-dimensional case is represented by rotating each figure about the axis through the origin and in the direction of B_o.

Before going further it is appropriate to consider the characteristics of each of the four wave modes.

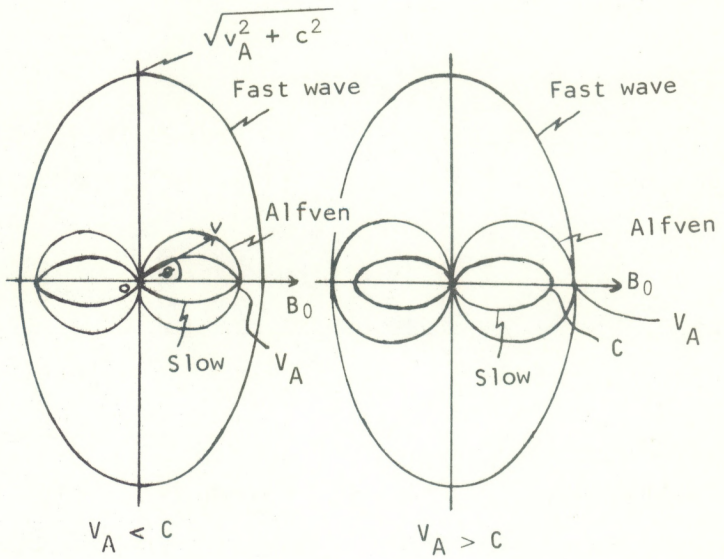

Figure 8. Friedrichs diagram (hodographs) for the two cases $V_A < C$ and $V_A > C$, after Ferraro (1966).

2.1.1 Magneto-Acoustic Mode

The magneto-acoustic wave arises when the velocity of the particles is in the direction of wave propagation and perpendicular to the magnetic field. In this case the magnetic pressure $B^2/2\mu$ must be added to the gas pressure P. The total pressure is then $P_T = P_o + B^2/2\mu$ and the wave speed is therefore

$$C_T = \{\frac{dP_T}{d}\}^{\frac{1}{2}} = \{\frac{d}{d\rho}(P_o + \frac{B^2}{2\mu})\}^{\frac{1}{2}} = \{C^2 + \frac{B_o^2}{\mu\rho_o}\}^{\frac{1}{2}} = \{C^2 + V_A^2\}^{\frac{1}{2}} \quad .$$

2.1.2 Alfvén Mode

The Alfvén mode is considerably different. Substituting the velocity $V_A \cos\theta$ back into our full set of differential equations we find for the changes in flow properties across the wavefront

and

$$dv_x = \pm \frac{dB_x}{\{4\pi\rho\}^{\frac{1}{2}}}$$

$$dv_z = d\rho = dp = dB_y = dv_y = 0 \ .$$

We see that this type of wave is purely transverse, since dv_z is zero. This means that (to first order) there is no change in pressure or density. Further, since the change in the magnetic field is perpendicular to the original field there is again, to first order, no change in the magnitude of the field but only a change in direction. As can be seen from the Freiderichs diagram, the Alfvén mode cannot propagate perpendicular to the magnetic field.

2.1.3 Fast and Slow Modes

The fast and slow modes are somewhat more complex, their characteristics being more strongly determined by the strength of the magnetic field. The velocity of these waves is given by the roots of (F2)

$$V^2_{F,Sl} = \tfrac{1}{2}\left\{C^2 + V_A^2 \pm \left[(C^2 + V_A^2)^2 - 4C^2 V_A^2 \cos^2\theta \right]^{\frac{1}{2}}\right\}$$

(Osterbrock, 1961). For the case of a very weak magnetic field $C >> V_A$ and the fast mode velocity is $V_F = C$, whereas for a very strong field $C << V_A$ and $V_F = V_A$. In both of these cases the velocity is independent of the direction of propagation. At intermediate values of the field strength the velocity is a weak function of direction. The most extreme variation of velocity with propagation direction occurs for the case $V_A = C \equiv V$. Then

$$V_F^2 = V^2 \{1 + \sin\theta\}.$$

Not only does the velocity of the fast mode vary with direction, but the nature of this mode also changes. With weak fields the material motion is longitudinal and the waves are essentially sound waves, whereas with strong fields the motion is perpendicular to the field and lies in the plane of $\overline{B}_o$ and of propagation so that the waves are magnetohydrodynamic in nature.

The slow mode is also affected by the magnetic field strength. Figure 9 shows that the slow mode cannot propagate across the magnetic field direction. In addition, for $C >> V_A$ (very weak fields) and $C << V_A$ (very strong fields) the slow mode can only propagate along the field. For intermediate fields we again have $C = V_A$ and the possible directions of propagation lie within a cone of half angle 27° (Osterbrock, 1961). For weak fields the speed is about V_A and the material motion is both perpendicular to the direction of propagation and in the plane of the magnetic field. For strong fields the speed is about C and the material motion is in the direction of the field.

2.1.4 Wave Magnitudes

We next turn our attention to the question of the magnitudes of the MHD waves generated by convection zone turbulence. Using the work of

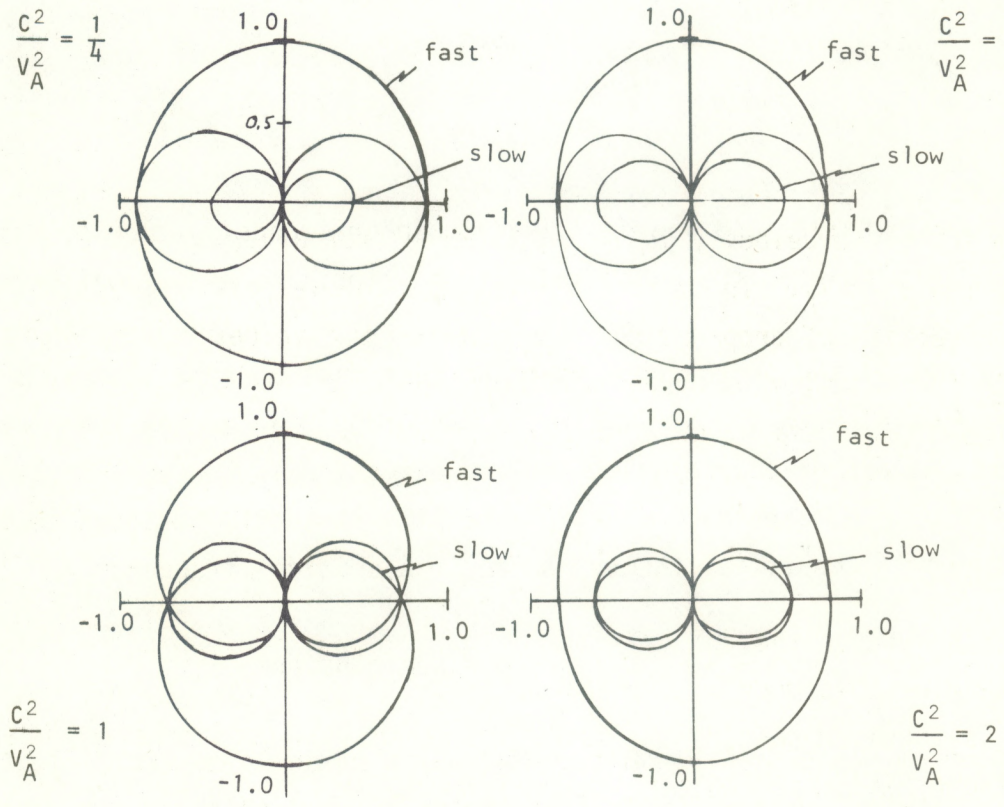

Figure 9. Friedrichs diagrams for various values of the sound to Alfven speed ratio, after Kunkel (1966).

Lighthill and Meecham, Osterbrock (1961) found that the spectrum of fast mode waves generated by turbulence in the convection zone is fairly flat, reaching a maximum at frequency

$$\nu_o = \frac{\langle v^2 \rangle^{\frac{1}{2}}}{l} = 1.2 \times 10^{-2} \text{ sec}^{-1}$$

where l is the turbulence scale length and $\langle v^2 \rangle^{\frac{1}{2}}$ is the root mean square of one component of the turbulent velocity. This ν_o corresponds to a period of T_o = 83 sec. He further found that essentially all the power generated is included between the frequencies

$$\nu_{min} = \tfrac{1}{4}\nu_o = 0.3 \times 10^{-2} \text{ sec}^{-1}$$

and

$$\nu_{max} = 4\nu_o = 4.8 \times 10^{-2} \text{ sec}^{-1}$$

which correspond to periods of

$$T_{max} = 21 \text{ sec}$$

and

$$T_{min} = 333 \text{ sec} \quad .$$

Using the Minnaert and van de Hulst atmospheric density models, Osterbrock has also calculated the sound and Alfvén velocities as a function of height in the solar atmosphere (table 2). Using the sound velocity of 6.3 km/sec at the photosphere, our shortest fast mode period of 21 sec gives a wavelength of some 132 km, or about 0.18 arcsec as seen from the Earth. We are of course using the approximation $V_F = C$ because at this level in the atmosphere $C >> V_A$ (table 2). It should be added that, according to acoustical theory, there is a critical frequency

$$\nu_c = \frac{C}{4\pi H} \qquad H = \text{scale height}$$

above which waves are transmitted and below which waves are reflected. For C=7 km/sec and H = 200 km (see table 3), we find that only waves with periods less than 332 sec (λ<2124 km) penetrate the photosphere and reach the chromosphere. We see, then, that we can most definitely have fast

*Table 2. Sound and Alfven Velocities in the Solar Atmosphere.**

Height (km)	Sound Velocity (km/sec)	Alfven Velocity (km/sec) B_o=2 gauss	Alfven Velocity (km/sec) B_o=50 gauss
2000	7.4	7.3	181
1500	7.0	2.6	65
1000	6.7	0.82	20
750	6.6	0.41	10.2
500	6.5	0.20	5.0
250	6.4	0.092	2.3
0	6.3	0.041	1.0
-100	6.4	0.025	0.62
-200	6.5	0.015	0.38
-300	6.7	0.010	0.25

*From Osterbrock (1961).

*Table 3. Scale Height as a Function of Height in the Solar Atmosphere.**

Height (km)	Scale Height (km)
1000	200
500	180
250	170
100	140
0	85
-100	140
-200	113
-300	148

*From Osterbrock (1961).

mode waves of considerably smaller wavelength than can be observed through the terrestrial atmosphere.

For Alfvén waves the case is somewhat different. An Alfvén wave propagating in the solar atmosphere will be damped because of two processes: Joule heating and frictional damping. The former is due

to collisions of electrons with positive ions and neutral atoms and the latter is due to collisions between positive ions and neutral atoms.

For an Alfvén wave propagating in the direction of the magnetic field, Osterbrock (1961) gives the distance in which the energy flux drops by a factor of e^{-1} because of Joule heating as

$$\zeta_1 = \frac{V_A^3}{4\pi^2\nu^2\{(c^2/4\pi\rho) + (\beta/\rho)\}} \qquad \text{(in emu units)}$$

where σ is electrical conductivity in emu units sec^{-1}, β is viscosity, and c is the speed of light. The same energy damping length due to frictional damping is

$$\zeta_2 = \frac{V_A}{4\pi^2\nu^2} \frac{1+\eta}{\eta\tau_\eta} \qquad \text{(in emu units)}$$

where η is the ratio of the mass densities of neutral atoms to ions and τ_η is the average time it takes an atom to lose its momentum in collisions with ions. The total damping length is then

$$\frac{1}{\zeta_o} = \frac{1}{\zeta_1} + \frac{1}{\zeta_2} \quad .$$

Osterbrock has calculated ζ_1 and ζ_2 for $\nu = 1.2\times10^{-2}$ sec^{-1}, which are shown in tables 4 and 5. Examination of these tables shows that Alfvén wave damping in the quiet sun (say B = 2 gauss) is very large in the photosphere and low chromosphere, and that surely any Alfvén waves generated in the convection zone would be effectively damped before reaching the visible surface. However, if we consider a plage or sunspot area, where a field strength of, say, 50 gauss is quite plausible, circumstances change. The Alfvén velocity will of course be larger, and the damping length therefore greater, as seen in tables 4 and 5. The result is that a small fraction, about e^{-1}, of energy flux carried by Alfvén waves incident on the bottom of the photosphere will penetrate through to the chromosphere. Once in the chromosphere, the damping is low enough

*Table 4. Joule Heating Damping Lengths for Alfven Waves.**

Height (km)	ζ_1 (km) B_o=2 gauss	B_o=50 gauss
1000	2.6×10^{4}	4.0×10^{8}
500	1.1×10^{2}	1.7×10^{6}
0	5.3×10^{-1}	8.2×10^{3}
-100	1.1×10^{-1}	1.8×10^{3}
-200	2.7×10^{-2}	4.2×10^{2}
-300	1.4×10^{-2}	2.2×10^{2}

* From Osterbrock (1961).

*Table 5. Frictional Damping Lengths for Alfven Waves.**

Height (km)	ζ_2 (km) B_o=2 gauss	B_o=50 gauss
1000	2.5×10^{4}	6.2×10^{5}
500	6.3×10^{3}	1.6×10^{5}
0	6.6×10^{3}	1.7×10^{5}
-100	7.4×10^{3}	1.9×10^{5}
-200	3.9×10^{4}	9.8×10^{5}
-300	1.3×10^{5}	3.3×10^{6}

*From Osterbrock (1961).

that the waves will pass essentially undamped to the corona.

Now, the magnetic fields that manifest themselves in plages and sunspots must be rooted firmly below the surface. Since the field lines are frozen to the fluid the convection zone turbulence should then push field lines about at the same time that fast mode disturbances are formed, and the resulting frequency spectrum of Alfvén waves created by the displacement of field lines should have much the same form as the acoustical spectrum, specifically:

$$\nu_o = \frac{\langle \nu^2 \rangle^{\frac{1}{2}}}{1} = 1.2 \times 10^{-2} \text{ sec}^{-1}$$

$$\nu_{min} = \tfrac{1}{4}\nu_o$$

$$\nu_{max} = 4\nu_o$$

and again T_o = 83 sec, T_{max} = 21 sec, T_{min} = 333 sec.

Using the velocities from table 2, then, we would expect to have Alfvén wavelengths as short as 21 km at z=0 km and 400 km at z = 1000 km.

These are the waves we have good physical reasons to expect might exist, but what are the smallest Alfvén waves that can propagate without being damped out within one wavelength? For B = 2 gauss, damping is, as we said, very strong. But for B = 50 gauss, we can calculate from damping lengths that the smallest Alfvén wave that can propagate is about T = 1 sec, ν = 1 sec^{-1} , λ = 1 km at z = 0 km height. Here we define a wave to be propagating if the wavelength is less than the damping length.

The slow mode presents a more difficult case. We know, however, that in the C > V_A limit the slow mode approaches being a purely transverse wave, with speed everywhere nearly equal to the Alfvén mode speed (fig. 9). Thus in areas with our assumed field strength of 50 gauss we might expect to see some slow mode waves of dimension identical to the dimensions calculated above for Alfvén waves. (Additionally, Osterbrock suggests that slow mode waves may be generated in the upper chromosphere by collisions between the fast mode wavefronts, but a quantitative analysis of the slow mode waves thus produced is beyond the scope of this paper.)

The final mode we will consider is the magneto-acoustic mode, which propagates perpendicular to the magnetic field with velocity $V' = (C^2 + V_A^2)^{\frac{1}{2}}$. The damping length for a sound wave, where we are using the "kinematic" viscosity β/ρ is (Wood, 1955)

$$\zeta_3 = \frac{3C^2\rho}{\beta 8\pi^2\nu^2} .$$

Now, from table 2 we can compute the wave velocity V', which is shown in table 6. Using our standard frequencies of 1.2×10^{-2}, 0.3×10^{-2},

Table 6. Acoustic Mode Speed V' as a Function of Height in the Solar Atmosphere

Height (km)	C(km/sec)	V_A km/sec		$V'=(C^2+V_A^2)$ (km/sec)	
		B_o=2G	B_o=50G	B_o=2G	B_o=50G
2000	7.4	7.3	181	10.4	179
1000	6.7	0.82	20	6.75	21.1
500	6.5	0.2	5.0	6.5	8.2
0	6.3	0.041	1.0	6.3	6.4

and 4.8×10^{-2} (justified later) we find, with viscosities from Osterbrock, the damping lengths shown in table 7. We can see that the viscosity damping length is very large, in agreement with Osterbrock's results for fast mode waves, and that acoustic waves will propagate essentially unhindered by viscosity effects. Other dissipative mechanisms that should be taken into account are Landau damping and stochastic acceleration, but Barnes (1966) and Sturrock (1966) have shown that these effects are small for propagation perpendicular to the field.

Using the velocities calculated we can easily obtain typical wavelengths for the acoustic mode waves. We can again use the frequencies

Table 7. Viscosity Damping Lengths for Acoustic Mode Waves.

Height (km)	μ/ρ (km^2/sec)	ζ_3 for $\nu=1.2\times10^{-2}sec^{-1}$ (km)	ζ_3 for $\nu=.3\times10^{-2}sec^{-1}$ (km)	ζ_3 for $\nu=4.8\times10^{-2}sec^{-1}$ (km)
1000	7.6×10^{-4}	1.1×10^{8}	1.7×10^{9}	6.6×10^{6}
500	4.6×10^{-5}	1.6×10^{9}	2.6×10^{10}	9.9×10^{7}
0	2.6×10^{-6}	2.6×10^{9}	4.1×10^{11}	1.5×10^{9}
		above for B_o=2 gauss		
		below for B_o=50 gauss		
1000	7.6×10^{-4}	3.2×10^{9}	5.0×10^{10}	1.9×10^{8}
500	4.6×10^{-5}	3.3×10^{9}	5.0×10^{10}	1.9×10^{8}
0	2.6×10^{-6}	2.7×10^{10}	4.2×10^{11}	1.6×10^{9}

ν_{min}, ν_o, and ν_{max} because we expect these waves might be generated by turbulence in the convection zone, and Osterbrock's derivation of the frequency spectrum did not indicate any preferred direction. In other words, we expect that convection zone turbulence might simultaneously generate fast mode disturbances in the radial direction, along the field, and acoustic mode disturbances that propagate perpendicular to the field. The results of our calculations are shown in table 8. As can be seen, the shortest acoustic wavelength of interest to this study is about 130 km at the base of the photosphere.

Table 8. Wavelengths for Acoustic Mode Waves Propagating With Velocity V'.

Height (km)	$\lambda@\nu_o$ (km)	$\lambda@\nu_{min}$ (km)	$\lambda@\nu_{max}$ (km)	V' (km/sec)
2000	863	3463	218	10.4
1000	560	2247	141	6.75
500	539	2164	136	6.5
0	522	2097	132	6.3
		above for B_o=2 gauss		
		below for B_o=50 gauss		
2000	1.48×10^4	5.9×10^4	3.7×10^3	179
1000	1.7×10^3	7.0×10^3	4.4×10^2	21.1
500	6.8×10^2	2.7×10^3	1.7×10^2	8.2
0	5.3×10^2	2.1×10^3	1.3×10^2	6.4

2.2 Observable Characteristics

We next consider the characteristics of these wave modes that lend themselves to optical observations.

2.2.1 Alfvén Mode

We have established that the velocity fluctuations in an Alfvén wave are perpendicular to the magnetic field, and we have restricted ourselves to Alfvén waves propagating along the (radial) field. (We are

of course ignoring active Sun features such as loops.) We would, therefore, expect to see horizontal motion manifested as either line-of-sight Doppler shifts or as horizontal displacements of ambient features being perturbed by passage of the wave. The amplitude of the horizontal displacement is

$$dx = T\ dv/2\pi$$

where dv is the amplitude of the associated velocity fluctuation and T the period of the wave. Following Hollweg (1972a) we can find dv as follows. The Poynting flux over one cycle of the wave is given by

$$S = \tfrac{1}{2}(c/4\pi)\ dE\ dB$$

where dE and dB are the amplitudes of the wave-caused electric and magnetic field fluctuations and c is the velocity of light. Further

$$dE = B_0\ (dv/c)$$

in a perfectly conducting medium, and from Faraday's law,[22] we have

$$dB = (kc/\omega)dE = (kB_0/\omega)dv$$

where $\omega/2\pi$ is the wave frequency and k is again the wave number. Combining yields

$$dv = B_0^{-1}\ (8\pi S\tfrac{\omega}{K})^{\frac{1}{2}}$$

and since ω/k is the Alfvén speed,

$$dv = 2(S/B_0)^{\frac{1}{2}}\ (\pi/\rho)^{\frac{1}{4}}$$

or alternatively,

$$dv^2 = 8\pi S\ V_A/B_0^2$$

which is easier for calculations. Now, finding the Poynting flux is a complex affair, but Hollweg (1972b) has shown that in the WKB limit[23]

$$S = (B_0^2/8\pi)\ (A^2/V_A)$$

where V_A is at height z = 0, and A is the velocity amplitude of a disturbance generating Alfvén waves.

Vitense (1953) has modeled the hydrogen convection zone and gives as root mean square turbulent velocities

Height (km)	$\langle v^2 \rangle^{\frac{1}{2}}$
-350	0.0
-400	0.5
-450	2.3
-525	2.1
-600	1.8
-700	1.5

Now, an rms velocity of about 2 km/sec corresponds to a velocity amplitude of about 3 km/sec, and an rms velocity of 0.5 km/sec corresponds to a velocity amplitude of about 0.6 km/sec. Using these values we can compute S, dv, and dx as shown in table 9.

We see from this table that we have velocities ranging from 1.3 to 29.3 km/sec and horizontal excursions ranging from 0.2 to 1.5×10^3 km. We will discuss how to observe these phenomena in section 2.3, but first we will undertake similar arguments and calculations for the acoustic and fast modes.

2.2.2 Fast Mode

Since we are considering only fast mode propagation along the field in a regime where $C > V_A$, we have essentially a sound wave propagating along a column of gas. According to acoustic theory (Ingard and Kraushaar, 1966), the temperature differential caused by such a wave, in the adiabatic case, is

$$\Delta T = (\gamma - 1) \frac{u}{C} T_o$$

where ΔT is the temperature difference, γ is the ratio of specific heats, u is the velocity of the disturbance causing the wave (a piston in classical theory), C is the sound speed, and T_o is the initial temperature. Taking $\gamma = 7/5$ (the generally accepted value for a diatomic gas; $\gamma_{H2} = 1.41$), u = A (the convection zone turbulent velocity amplitude), and $T_o = 6000°K$ (a reasonable photospheric value), we find ΔT as shown in table 10.

Table 9. Poynting Flux, Velocity Fluctuation, and Horizontal Displacements of Alfven Waves for Various Values of z, A, V_A, and B_o.

					Poynting Flux	Velocity Fluctuation	Horizontal Displacement			
z (km)	A (km/sec)	V_A (km/sec)	B_o (gauss)	ρ (g/cm^3)	S (erg $cm^{-2}sec^{-1}$)	dv (km/sec)	dx for T=21sec (km)	dx for T=83 sec (km)	dx for T=333sec (km)	dx for T=1 sec (km)
-400	0.6	0.0082	2	$3.1x10^{-7}$	$6.98x10^5$					
-425	3	0.0082	2	$3.2x10^{-7}$	$1.74x10^7$					
-400	0.6	0.2	50	$3.1x10^{-7}$	$1.79x10^7$					
-425	3	0.2	50	$3.2x10^{-7}$	$4.48x10^8$					
0		0.041	2		$1.70x10^7$	6.5	21.17	85.8	344.5	1.03
0		1.0	50		$1.70x10^7$	1.3	4.3	17.2	68.9	0.20
500		0.2	2		$1.70x10^7$	14.5	4.8	191.4	768.5	2.30
500		5.0	50		$1.70x10^7$	2.9	9.7	38.3	153.7	0.46
1000		0.82	2		$1.70x10^7$	29.3	97.8	386.7	1500	4.66
1000		20	50		$1.70x10^7$	5.8	19.4	76.7	307.4	0.92

Table 10. Temperature Differential Due To Fast Mode Waves.

u(km/sec)	C(km/sec)	ΔT(°K)
0.6	6.5	240
3.0	6.5	1200

Now, from Boltzmann we know that the probability of finding an electron in an atomic energy state varies with the temperature as

$$\exp(-\chi/KT)$$

where χ is the excitation potential in electron volts and K is Boltzmann's constant = 1.38×10^{-16} erg/°K. For H-alpha χ = 1.88 eV, and so for 6000°K, 6000 + 240°K, and 6000 + 1200°K, (ΔT's from table 10), we have the following "Boltzmann probabilities" P:

T	P
6000	0.0302
6240	0.0334
7200	0.0550

We might expect then to see an increase of brightness in H-alpha of between 10 and 90 percent due to the increased number of electrons making downward transitions from their excited states. This result is consistent with, although lower in magnitude than, the result obtained by Kahn (1961) who attacked a similar problem using a somewhat different method.

2.2.3 Magneto-Acoustic Mode

The magneto-acoustic mode, being essentially a hybrid sound mode, will behave similarly. Since the temperature variation ΔT goes as u, the velocity of the exciting mechanism, and since we have postulated convection zone turbulence to be responsible for both the fast and acoustic modes, we would expect that the acoustic mode may produce similar brightenings.

Additionally, however, the acoustic mode will cause motion not only of gas particles but also of magnetic field lines as the compressions

and rarefactions propagate across the disk. If we have solar features that outline the field structure, for example, the "feet" of prominences (observed, e.g., on the limb in H-alpha) we should be able to see the edge of this feature shift back and forth with time. The magnitude of this displacement is easy to calculate. It will be

$$dx = T \frac{dv}{2\pi}$$

where dv is now the velocity of the initial disturbance and T is the period. In this case, dv = u. Table 11 shows a computation of dx using the same velocity amplitudes, i.e., u = 0.6 and 3.0 km/sec. As the table shows, the waves under consideration could be expected to produce displacements of between 2 and 159 km.

Table 11. Horizontal Displacement Caused By Acoustic Mode Waves.

u(km)	dx(km) T=21 sec	dx(km) T=83 sec	dx(km) T=333 sec
0.6	2.00	7.93	31.81
3.0	10.08	39.64	159.07

2.3 Observation of MHD Waves

In section 2.2 we discussed the MHD wave equations and calculated the magnitudes of some characteristics of the MHD waves which we would expect to be generated by convection zone turbulence. In this section we will briefly consider the observation of these waves.

2.3.1 Alfvén Mode

We saw in section 2.2 that Alfvén waves will cause motion in the field lines along which they propagate. As shown in figure 10, these motions will be seen by an observer as either horizontal displacements or as Doppler shifts. The amplitudes of the horizontal displacements from table 9 range from 2.7×10^{-4} to 2.0 arcsec, as shown in table 12.

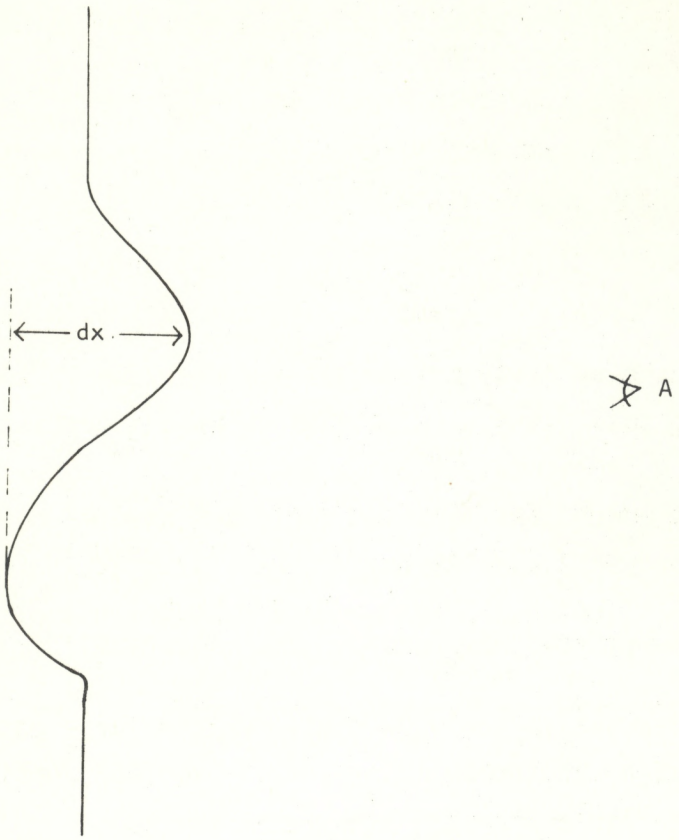

Figure 10. Alfven wave propagating along field line. Observer at A will see a Doppler shift, whereas observer at right angles to A (i.e., looking into paper) will see horizontal displacement dx.

Table 12. Alfven Wave Horizontal Displacements.

Height (km)	B_o (gauss)	dx T=21 sec (arcsec)	dx T=83 sec (arcsec)	dx T=333 sec (arcsec)	dx T=1 sec (arcsec)
0	2	2.9×10^{-2}	1.2×10^{-1}	4.7×10^{-1}	1.4×10^{-3}
0	50	5.9×10^{-3}	2.3×10^{-2}	9.5×10^{-2}	2.7×10^{-4}
500	2	6.6×10^{-3}	2.6×10^{-1}	1.06	3.1×10^{-3}
500	50	1.3×10^{-2}	5.2×10^{-2}	2.1×10^{-1}	6.3×10^{-4}
1000	2	1.3×10^{-1}	5.3×10^{-1}	2.0	6.3×10^{-3}
1000	50	2.6×10^{-2}	1.0×10^{-1}	4.2×10^{-1}	1.3×10^{-3}

The velocity fluctuations dv will give rise to Doppler shifts. Doppler shift is of course given by

$$\frac{\Delta\lambda}{\lambda} = \frac{dv}{c} \qquad \text{whence } \Delta\lambda = \frac{\lambda dv}{c}$$

where c is the speed of light and λ is the wavelength of the line being observed. For H-alpha, for example, the Doppler shifts corresponding to the velocity fluctuations listed in table 9 for Alfvén waves are:

Height (km)	B_o Gauss	$\Delta\lambda$(A)
0	2	1.42×10^{-1}
0	50	2.84×10^{-2}
500	2	3.17×10^{-1}
500	50	6.34×10^{-2}
1000	2	6.40×10^{-1}
1000	50	1.26×10^{-1}

These Doppler shifts are very small but are large enough to be observed with existing instrumentation (Billings, 1963) providing adequate resolution is available.

2.3.2 Fast Mode

Detecting the fast mode involves us in a more complex mathematical problem. The brightness increases we have postulated are certainly enough to detect, but the spatial extent of the brightenings is not clear, nor is the temporal duration. These will be functions of the local thermal relaxation time and the local radiative processes involved in forming the line being studied, and line-of-sight complexities due to out-of-phase brightenings may also be important. These problems will have to be studied in detail before any conclusions regarding the detectability of fast mode waves can be reached.

2.3.3 Magneto-Acoustic Mode

The acoustic mode offers more promise. The horizontal displacements calculated in the preceding section are, in arcseconds:

u (km/sec)	dx (T=21 sec)	dx (T-83 sec)	dx (T=333 sec)
0.6	2.7×10^{-3}	1.1×10^{-2}	4.4×10^{-2}
3.0	1.4×10^{-2}	5.5×10^{-2}	2.2×10^{-1}

If a suitable boundary is available, as for example the prominence "feet" suggested earlier, then a telescope with suitably high resolution should be able to detect this motion.

We are now in a position to understand what "suitably high resolution" means. From the calculations we can see that some tenths to hundredths of an arcsecond are required. This resolution, however, was shown in the first section to be unobtainable from ground-based observatories because of the perturbing effects of the terrestrial atmosphere. The alternative, then, is to utilize a large orbiting solar observatory. To meet these resolution requirements we would need a reflecting telescope of between 1 and 10 m aperture, depending on wavelength (see fig. 11). The total length of such a package would be large, which would allow sufficient room for accessories such as stigmatic spectrographs, spectroheliographs, magnetographs, cameras, and filters. Such an instrument is feasible. NASA has recently announced it is letting preliminary contracts for an orbiting telescope with a 10-m mirror, to be capable of launch in 1980 aboard a space shuttle into a 483 x 402 mile orbit (Aviation Week, 1973).

3. SUMMARY

We have seen that the study of the Sun in all its aspects is an important endeavor, and have suggested how the aspect of MHD wave propagation is an important study in its own right. We have shown that the hydrogen convection zone is a region of great turbulence, and that this turbulence extends to and is visible in the photosphere in the form of granulation. In addition, we have shown, from basic continuity equations, other work in the field, and hypotheses and calculations of our own that the various modes of MHD waves generated by convective turbulence display the following characteristics.

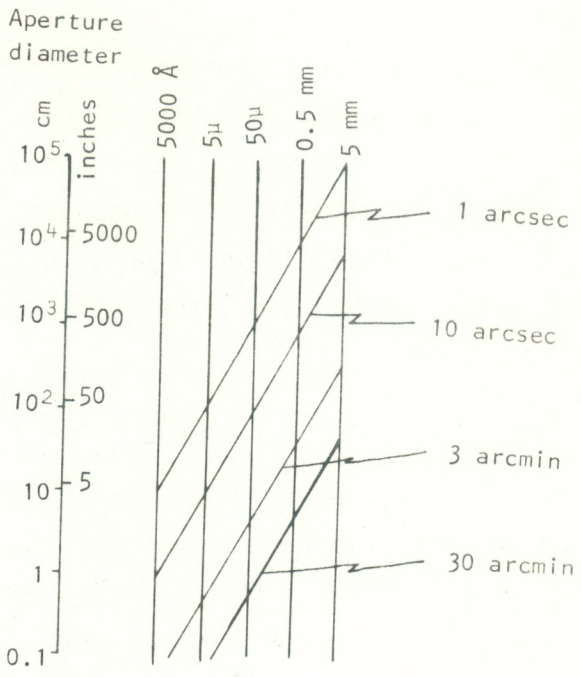

Figure 11. Resolution of a reflecting telescope as a function of aperture diameter and wavelength. From National Academy of Science (1966).

3.1 Fast Mode

Fast mode waves were shown to be strongly dependent on the strength of the ambient magnetic field. For weak fields $V_F = C$ and the material motion is longitudinal: essentially a sound wave. For strong fields $V_F = V_A$ and the material motion is perpendicular to the magnetic field. Using the frequency spectrum for fast mode waves generated by convection zone turbulence derived by Osterbrock, we found that the expected frequency range was of the order 0.3×10^{-2} sec^{-1} to 4.8×10^{-2} sec^{-1}. This, together with our condition that $V_F = C$ (as justified in the text) and Osterbrock's calculations of local sound speeds, leads to the conclusion that the shortest fast mode "wavelength" produced by turbulence would be some 132 km, or about 0.18 arcsec.

Now, in this weak field case, the fast mode approximates a sound wave, and in the case of radial fields we have essentially the case of a sound wave propagating in a column of gas. Under these conditions we

showed that there should be local brightenings due to local increases of temperature. We did not, however, determine the temporal duration or spatial extent of these brightenings. These are functions of the local thermal relaxation time, local radiative processes involved in formation of the emission line being studied, and line-of-sight complexities due to out-of-phase brightenings; as such, they are of necessity left to a later work.

3.2 Slow Mode

The characteristics of the slow mode, as of the fast mode, were shown to depend on the relative field strength. For strong fields $V_{sl} = C$ and the material motion is in the direction of the field, but for our weak field case $V_{sl} = V_A$, and the material motion is perpendicular to the direction of propagation. In addition, we saw from the hodographs that the slow mode cannot propagate across the field.

Now, slow mode damping is strong in the lower solar atmosphere, but in areas of enhanced field strength - perhaps 50 gauss - we might see some slow mode waves of the same dimension as calculated for Alfvén waves. However, since most slow mode waves may be generated by collisions between fast mode wavefronts, a topic beyond the scope of this paper, the slow mode was not pursued further.

3.3 Magneto-Acoustic Mode

The magneto-acoustic mode was shown to be a "hybrid" mode in which material motion is in the direction of wave propagation and perpendicular to the field. This mode was demonstrated to propagate essentially undamped, and assuming the Osterbrock frequency spectrum yielded a shortest "wavelength" of some 130 km at the base of the photosphere.

This mode was hypothesized, along with the fast mode, to cause brightness fluctuations (since it is a hybrid sound wave), but in addition was hypothesized to create fluctuations in field lines as compressions and rarefactions propagate across the disk. These effects were calculated to be between 2 and 159 km (2.7×10^{-3} to 2.2×10^{-1} arcsec) for the frequencies

of interest. The "feet" of prominences, where fields of various strengths are assumed to exist and which stand out well on the limb, were suggested as opportune locations in which to search for these effects.

3.4 Alfvén Mode

The Alfvén mode was shown to be purely transverse, with no change (to first order) produced in local pressure or density and with a change produced only in the direction but not in the magnitude of $\underline{B}$. The Alfvén mode was also shown to be incapable of propagating perpendicular to $\underline{B}$.

The Osterbrock frequency spectrum was assumed to apply also to Alfvén waves produced by convective turbulence, and a corresponding minimum "wavelength" of 21 km at the base of the photosphere was calculated. Calculations for moderate field strengths (about 2 gauss) showed that all Alfvén waves would be quickly damped, but similar calculations for stronger fields (about 50 gauss) showed that in active regions or other areas of enhanced magnetic flux an appreciable fraction of the Alfvénic energy flux would survive and be transmitted to the corona.

Calculations of the local velocity fluctuations (shown to be perpendicular to $\underline{B}$) produced by Alfvén waves provided magnitudes of 1.3 to 29.3 km/sec for the frequency spectrum of interest, which correspond to horizontal displacements of 0.2 to 1.5×10^{3} km (2.7×10^{-4} to 2.0 arcsec) and Doppler shifts of 6.4×10^{-1} to 2.8×10^{-2} Å. Again, the "feet" of prominences may be prime areas in which to detect these effects.

3.5 Remarks

As can be seen from the calculations performed, the magnitudes of the effects expected to be generated by MHD waves in the relevant frequency spectrum are quite small. This immediately restricts our possible observing methods since, as was shown in the introduction, atmospheric limitations are of the order of 0.5 arcsec. It is clear then that orbiting telescopes are needed. There are, however, several points that were beyond the scope of this treatise which should be examined in detail before a search for these wave modes is carried out.

First, the brightness fluctuations postulated to be generated by fast mode waves should be examined with attention paid to local thermal relaxation times, line formation processes, and possible additional brightness fluctuations caused by density fluctuations. Density-caused brightness fluctuations could either be in phase or out of phase with thermal brightness fluctuations, as could brightness fluctuations in other volume elements in the line of sight, so that the net effect at 1 AU could be to produce no overall fluctuations. In addition, it is not clear how displacements in field lines and Doppler shifts due to Alfvén waves would be observed in the lower solar atmosphere; limb studies are clearly in order and the areas over active regions and prominence "feet" would seem to be the most likely target areas, but further study of field orientation and mass distribution is needed. Also, a more accurate determination of Poynting flux would lead to a better approximation of expected displacements and Doppler shifts.

One additional interesting piece of information is apparent from this report. We have seen that outward energy flux increases in some wave modes with increasing field strength. Chapman (1974) indicates that the chromospheric network may contain small bundles of high field strength, and Withbroe (1974) has indicated that the chromospheric network is visible in all lines up to just above 1×10^{6}°. Thus it seems plausible that energy in the form of MHD waves may be channeled upward through the network, and network areas may therefore be excellent areas in which to search for these waves.

Sunspot umbrae may also be excellent locations to study these waves. Giovanelli has recently found waves with 180-sec periods appearing in umbrae and moving outward through penumbrae (Giovanelli, in press). This period falls exactly within our postulated frequency spectrum, and the strong fields in sunspots would of course lead to a strong wave-channeling effect.

In any event, further studies of turbulence-generated MHD waves will certainly be valuable. One type of benefit might be increased understanding of solar processes. For example, if sufficient subphotospheric energy in the form of MHD waves is channeled in flux tubes to the corona,

existing coronal instabilities could be triggered. We could perhaps imagine that energy flux coming up both legs of a loop-shaped magnetic structure seated high over an active region might meet at the top, thus triggering an instability which could itself be the primary flare-triggering mechanism (fig. 12). A more complete understanding of MHD wave propagation in the lower solar atmosphere might therefore help unlock such basic solar secrets as the primary flare mechanism.

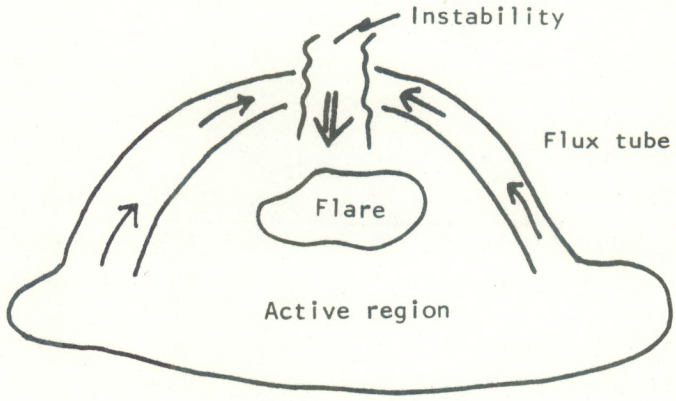

Figure 12. Possible flare triggering mechanism.

4. ACKNOWLEDGMENTS

The author expresses his appreciation to Dr. Joseph Hollweg, University of Colorado, for his continual guidance and helpful suggestions, and to Drs. Sayvetz, Billings, and Speiser for their careful reading of the manuscript and their helpful comments.

5. FOOTNOTES

[1] Solar activity runs in cycles roughly 11 years in length. Overall, however, the change in luminosity due to activity is very small, and is much too small to be observed as fluctuations in intensity of a distant star. Activity can only be studied on a star which is close enough not to appear as a point source.

[2] The Hertzsprung-Russell diagram (see fig. 13) is a classic presentation of observational data. When stellar temperature is plotted versus luminosity, the observed stars fall into evolutionary tracks, or sequences. Our Sun is presently in what is called the main sequence, and as such is spectroscopically a quite ordinary star.

[3] For example, Dr. Percy Carr at Iowa State University is assembling statistical and experimental evidence that solar induced geomagnetic storms cause some breeds of homing pigeons to become so lost that they are unable to return to their lofts. The Division of Biological Sciences, Cornell University, is doing similar work.

[4] An unusually energetic series of solar flares in August 1972 created a space radiation hazard so severe that, had an astronaut been exposed to the entire storm, severe incapacitation or death could have resulted (McKinnon, 1972).

[5] In 1868 while observing an eclipse in India, the French astronomer J. Janssen discovered a helium line in the chromospheric spectrum. Helium was not discovered on Earth until Sir William Ramsey found it in 1894.

[6] Bengt Edlen won gold medals from several leading scientific institutions for his work in 1944 on coronal emission lines.

[7] Resonance lines arise from atomic transitions that connect the ground state of an atom with the first excited state. These are the last lines visible as a discharge producing the spectrum of the atom fades away.

[8] The transition region is the narrow layer between the chromosphere and corona. The temperature minimum in the solar atmosphere occurs at the base of the transition region.

[9] Rotational energy of a molecule can be expressed in terms of its principal moments of inertia I_a, I_b, I_c and angular moments P_a, P_b, P_c, (where a, b, and c represent the principal axes of the momental ellipsoid):

$$E_{rot} = \sum_{a}^{c} \frac{P_i^2}{2I_i} \quad .$$

The rotational motions are quantized and the total angular momentum P can only take the values

$$P = \{J(J+1)\}^{\frac{1}{2}} \hbar \quad , \qquad (\alpha)$$

J=0 or integer. Also, the component of P in a fixed direction in space is quantized according to

$$P_z = M \hbar$$

where M can take the 2J+1 values M = J, J-1, ...-J. For a linear molecule, $I_a = 0$ and $I_b = I_c \equiv I$, and

$$E_{rot} = \frac{p^2}{2I}$$

whence, from eq. (α), we obtain the characteristic energies

$$E_j = \frac{\hbar^2 J(J+1)}{2I} = hBJ(J+1) \qquad \text{where } B = \hbar/(2I) \quad .$$

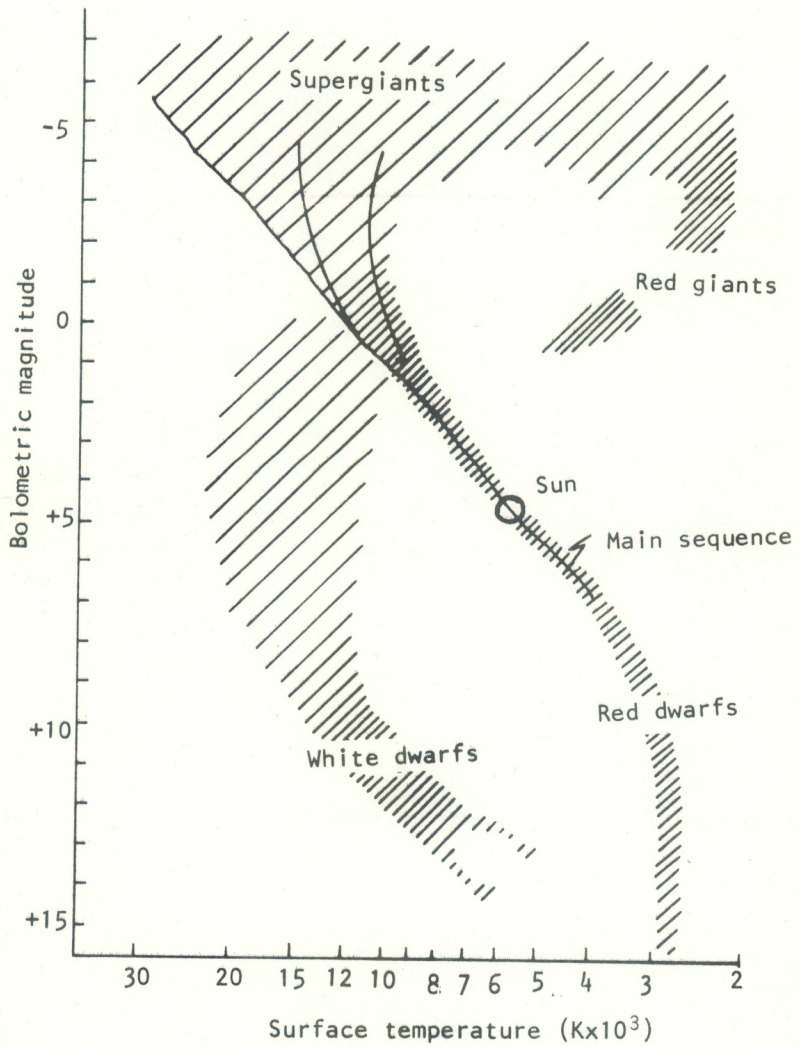

Figure 13. Hertzsprung - Russell diagram, showing the relationship of the Sun to other stars. After Brandt (1966).

The molecule can absorb radiation with J increasing by integral steps. The selection rule for absorption is J→ J+1, giving rise to absorption frequencies

$$n = 2B(J+1) \quad .$$

The rotational spectra, or rotational bands, of a molecule then consist of equally spaced lines, the lowest frequency being 2B.

[10] A McLaurin series is a Taylor's series of the form

$$f(x) = \sum_{n=0}^{\infty} \frac{f^n(a)}{n!} (x-a)^n$$

for the case a = 0.

[11] Theorem of the mean

Given a continuous function f, and f'(x) exists and $a \leq x \leq b$, then there is a c such that

$$f'(c) = \frac{f(b) - f(a)}{b - a}$$

where $a < c < b$

[12] Consider a bubble of material in the Sun. If this bubble is moved upward a distance dr, the change in temperature of the bubble is $dr|dT/dr|_{ad}$, where $|dT/dr|_{ad}$ is the adiabatic temperature gradient. (We assume the bubble does not exchange heat with its surroundings.) The surrounding material has a temperature difference of $dr|dT/dr|_{str}$, where $|dT/dr|_{str}$ is the structural gradient in the Sun. If $|dT/dr|_{str} > |dT/dr|_{ad}$, which is the Schwarzschild instability criterion, the bubble will cool less than the surrounding material, and, since it is in pressure equilibrium, must be less dense. The buoyancy force therefore pushes the bubble upward and an instability results.

[13] The effective temperature of a star is the temperature of a black body of equal radius that produces the same total luminosity.

[14]

$$\frac{dP}{dr} = \frac{\rho GM(r)}{r^2}$$

where r = radial distance, P = pressure, ρ = density, G = constant of gravitation, M(r) = mass contained within a spherical shell or radius r.

[15] Scale height is defined by

$$\frac{N}{N_o} = \exp(-x/H)$$

where N = density at x, x = height in atmosphere, N_o = density at x = 0, H = scale height.

[16] Called Fraunhofer lines.

[17] The line emitted by hydrogen as the electron drops from the third to the second principal orbit.

[18] A sunspot group and its associated plage.

[19] Assume a hydrogen ion with positive charge e located at r = 0, with U(r) the electric potential. Then the density of positive charge will be a Boltzmann distribution

$$\rho_+ = n_e\, e(\exp(\frac{Ue}{KT}))^{-1}$$

and for negative charge

$$\rho_- = n_e e \exp(\frac{Ue}{KT}) \ .$$

Using Poisson's equation in its general form $\Delta^2\theta = f(x,y,z)$ gives (Margenau and Murphy, 1956)

$$\Delta^2 u = 4\pi n_e e \{\exp(\frac{Ue}{KT}) - \exp(\frac{Ue}{KT})\} \ .$$

This a nonlinear differential equation which must be integrated numerically or else fudged (Reitz and Milford, 1967). An approximate solution -- and one that is rigorous at high temperatures -- can be used by assuming Ue/KT >> 1. (If T ~ 10^6°K then Ue/KT $\leq$ 2 x 10^{-9}/r, which is << 1 for all r greater than atomic radii, so we're safe.) Then each exponential can be represented by the first two terms of a McLaurin expansion. Solving gives

$$U = (\frac{e}{r})\exp\{-(\frac{r}{D})\} \qquad \text{(Debye Potential)}$$

where

$$D = (\frac{KT}{8\pi n_e e^2})^{\frac{1}{2}} \ .$$

D is called the Debye length and is the distance from an ion at which the electric field is significantly less than the inverse square electric field because of the shielding of neighboring ions. D is therefore the maximum distance from an ion at which the electric field of the ion is significant and is of the order of, at most, a few millimeters in the corona (Billings, 1966).

[20] The current due to an electric field E can be written

$$\sigma E = j + \frac{e}{\nu m_e}\, \underline{j} \times \underline{B}$$

where σ = conductivity and ν = number of collisions/sec undergone by electrons with charge e and mass m_e. Therefore,

$$\sigma \underline{E} \cdot \underline{j} = j^2 \ .$$

But $\underline{E} \cdot \underline{j}$ is the rate at which the electric forces work during the flow of current. Therefore, j^2/σ is called Ohmic dissipation, or Joule heating.

[21] Stokes' theorem: the line integral of a vector around a closed curve is equal to the integral of the normal component of its curl over any surface bounded by the curve

$$\oint F \cdot dl = \int \text{curl } F \cdot n \, da$$

[22] Curl $\underline{E} = -\frac{\partial B}{\partial t}$, in differential form

[23] For the WKB limit to hold, the scale height for the Alfvén speed must be greater than the wavelength. Using the Alfvén speeds listed in table 2 for a 2 gauss field at a height of 1500 km, the wavelength of a disturbance with frequency 10^{-2} sec^{-1} would be 260 km, about equal to the scale height for the Alfven speed. So, for the frequencies in question we can use the WKB approximation in the lower solar atmosphere.

6. REFERENCES

Alfven, H., and C. Falthammar (1963), *Cosmical Electrodynamics*, Clarendon Press, Oxford.

Aviation Week and Space Technology (1973), 99, p. 51, July 2.

Barnes, A. (1966), Collisionless damping of hydromagnetic waves, *Phys. Fluids*, 9, 1483-1495.

Belcher, J., and L. Davis (1971), Large amplitude Alfven waves in the interplanetary medium, *J. Geophys. Res.* 76, 3534-3563.

Billings, D. (1963), Spectroscopic limitation on coronal heating mechanisms, *Astroph. J.* 137, 592-599.

Billings, D. (1966), *A Guide to the Solar Corona*, Academic Press, New York.

Brandt, J. (1966), *The Sun and Stars*, McGraw-Hill, New York.

Chapman, G. (1974), On the nature of the small scale solar magnetic field, *Astroph. J.* 191, 255-259.

Ferraro, V., and C. Plumpton (1966), *An Introduction to Magneto Fluid Mechanisms*, Clarendon Press, Oxford.

Feynman, R. (1963), *Lectures on Physics*, 1, Addison Wesley Pub. Co., Reading, Pa.

Gibson, E. (1973), *The Quiet Sun*, Natl. Aeronautics and Space Admin., Washington, D.C.

Giovanelli, R. (in press), Chromospheric oscillations and waves in sunspots and active regions, IAU Symp. 56, Sept. 1973.

Hines, C. (1973), Comments on "A test of an apparent response of the lower atmosphere to solar corpuscular radiation", *J. Atmos. Sci.*, 30, 734-744.

Hollweg, J. (1972a), Alfvenic motions in the solar atmosphere, *Astroph. J.* 177, 255-259.

Hollweg, J. (1972b), Supergranulation driven Alfven waves in the solar chromosphere, *Cosmic Electrodyn.* 2, 423-444.

Hollweg, J. (1972c), Private communication.

Ingard, U., and W. Kraushaar (1966), *Introduction to Mechanics, Matter and Waves*, Ch. 21, Addison Wesley Pub. Co., Reading, Pa.

Kahn, F. (1961), Sound waves trapped in the solar atmosphere, *Astroph. J.* 134, 343-346.

Kunkel, W. (1966), *Plasma Physics in Theory and Application*, McGraw-Hill, New York.

Margenau, H., and G. Murphy (1956), *The Mathematics of Physics and Chemistry*, Van Nostrand, Princeton, N.J.

Markson, R. (1971), Considerations regarding solar and lunar modulation of geophysical parameters, *Pure and App. Geophys.* 84, 161-202.

McKinnon, J. (1972), August 1972 solar activity and related geophysical effects, NOAA Tech. Memo. ERL/SEL-22, Dept. of Commerce, Boulder, Colo.

Menzel, D. (1961), The theory of atmospheric seeing, Proc. of the International Symposium of Solar Seeing, Feb. 1961, Consiglio Nazionale delle Ricerche, Rome, pp. 25-30.

Mustel, E. (1972), Effect of solar particle flux on the lower atmosphere, *Astr. Sovet Akad. Nauk SSSR, Nauch.Inform.* SSSR (1972), no. 24, 5-55.

Natl. Academy of Science (1966), *Space Research Directions for the Future,* Publica. 1403, Natl. Academy of Science, Washington, D.C.

Osterbrock, D. (1961), The heating of the solar chromosphere, plages, and corona by MHD waves, *Astroph. J.* 134, 347-387.

Reitz, J., and F. Milford (1967), *Foundation of Electromagnetic Theory,* Addison Wesley Pub. Co., Reading, Pa.

Roberts, W. (1973), New evidence for effects of variable solar corpuscular emission on the weather, *Rev. Geophys. and Space Phys.* 11, 731-740.

Spitzer, L. (1962), *Physics of Fully Ionized Gases,* Interscience Publishers, New York.

Sturrock, B. (1966), Stochastic acceleration, *Phys. Rev.* 141, 186-191.

Vitense, E. (1953), Die Wasserstoffkonvektionszone der Sonne, *Zeits. Astrophysik,* 32, 135-164.

Wilcox, J. et al. (1973a), Solar magnetic sector structure, *Science* 180, 185-186.

Wilcox, J. et al. (1973b), Influence of solar magnetic structures on terrestrial atomospheric vorticity, SUIPR Rept. No. 530, Institute for Plasma Research, Stanford University, Stanford, Calif.

Wilcox, J. (1973c), Solar activity and the weather, SUIPR Rept. No. 544, Institute for Plasma Research, Stanford University, Stanford, Calif.

Withbroe, G. (1974), Ultraviolet scanning polychrometer, presented at AAS Solar Physics Division Meeting, Univ. of Hawaii, Honolulu, January.

Wood, A. (1955), *A Textbook of Sound,* B. Bell and Sons, London.

7. BIBLIOGRAPHY

Alfven, H. (1947), Granulation, magnetohydrodynamic waves, and the heating of the solar corona, *Monthly Notices Roy. Astron. Soc.*, 107, 211-219.

Dungey, J. (1958), *Cosmic Electrodynamics*, Cambridge Univ. Press, Cambridge.

Hollweg, J. (1971), Density fluctuations driven by Alfven waves, *J. Geophys. Res.* 76, 5155-5161.

Hollweg (1973), Alfven waves in the solar wind, *J. Geophys. Res.* 78, 3643-3652.

Hollweg, J. (1973), Alfven waves in a two fluid model of the solar wind, *Astrophys. J.* 181, 547-566.

Kuiper, G. (1953), *The Sun*, Univ. of Chicago Press, Chicago.

Kuperus, M. (1969), The heating of the solar corona, *Space Sci. Rev.*, 9, 713-737.

Ortner, J., and H. Maseland (1965), *Introduction to Solar Terrestrial Relations*, D. Reidel Pub. Co., Dordrecht.

Piddington, J. (1956), Solar atmospheric heating by hydromagnetic waves, *Monthly Notices Roy. Astron. Soc.*, 116, 314-323.

Thompson, W. (1962), *Introduction to Plasma Physics*, Pergamon Press, New York.